TSUNAMI INTERACTION WITH COASTLINES AND ELEVATION PREDICTIONS

By

JAMES ROBERT HOUSTON

A Dissertation Presented to the Graduate Council of
The University of Florida
In Partial Fulfillment of the Requirements for the
Degree of Doctor of Philosophy

UNIVERSITY OF FLORIDA

1978

ACKNOWLEDGMENTS

The writer wishes to express his sincere gratitude to his supervisory committee chairman, Professor Knox Millsaps, and co-chairman, Professor Joseph Hammack, for their support and efforts to provide him the opportunity to complete his studies at the University of Florida.

A special debt of gratitude is owed to Dr. R. W. Whalin, Chief of the Wave Dynamics Division, Hydraulics Laboratory, U. S. Army Waterways Experiment Station for his encouragement and active support during the research and preparation periods of this dissertation.

The writer wishes to thank Professor Umit Unluata for the insight he provided and for organizing a supervisory committee prior to his departure from the University. Appreciation also is extended to Dr. D. L. Durham for many helpful discussions at the Waterways Experiment Station.

The research upon which this dissertation is based was funded by the Pacific Ocean Division of the U. S. Corps of Engineers and the Federal Insurance Administration of the Department of Housing and Urban Development through the Office of the Chief of Engineers.

TABLE OF CONTENTS

	Page
ACKNOWLEDGMENTS	ii
KEY TO SYMBOLS	v
ABSTRACT	viii
CHAPTER I: INTRODUCTION	1
Tsunamis	1
Objective and Scope of Study	2
CHAPTER II: TSUNAMI INTERACTION WITH THE HAWAIIAN ISLANDS	4
Introduction	4
Governing Equations	7
Finite Element Model	12
Numerical Grid	21
Model Verification	25
CHAPTER III: TSUNAMI INTERACTION WITH CONTINENTAL COASTLINES	43
Introduction	43
Governing Equations	45
Finite Difference Model	48
Model Verification	51
CHAPTER IV: ELEVATION PREDICTIONS	58
Hawaiian Island Predictions	58
Introduction	58
Interpolation of Recent Historical Data	61
Time Period Analysis	63
Reconstruction of Historical Data	65
Frequency of Occurrence Distribution	69
Results	71

Page

West Coast of the United States Predictions 75

Introduction 75
Tsunami Occurrence Probabilities 77
Use of Deterministic Numerical Models 80
Effect of the Astronomical Tides 85
Comparison with Local Observation Predictions . . 88

CHAPTER V: CONCLUSIONS 95

APPENDIX: SUPERPOSITION OF LARGE TSUNAMIS AND ASTRONOMICAL TIDES 97

REFERENCES 99

BIOGRAPHICAL SKETCH 105

KEY TO SYMBOLS

a	Wave amplitude
b_o	Incident wave amplitude
$b(\omega)$	Amplitude of frequency component ω
C	Chezy's coefficient
C_m	Amplitude of m^{th} tidal coefficient
D	Period of time
f	Frequency of occurrence
$\vec{F}$	External force vector
$F( )$	Functional
g	Acceleration of gravity
h	Water depth
H_{avg}	Average runup, meters
H_m	Hankel function of first kind of order m
i	$(-1)^{1/2}$
I	Tsunami intensity
j	Integer
k	Wave number
$[K]$	Coefficient matrix
L	Wavelength
m	Integer
n	Unit normal vector
n_m	Manning's coefficient

$n(\ )$	Frequency of occurrence
N	Interpolation function
P	Pressure
$\vec{q}$	Velocity vector
$\{Q\}$	Total load vector
r	Spherical coordinate
t	Time
T	Wave period
u	Velocity component in x-direction
v	Velocity component in y-direction
w	Velocity component in z-direction
x	Cartesian coordinate
Δx	Small increment in x
y	Cartesian coordinate
Δy	Small increment in y
z	Cartesian coordinate (vertical direction)
α	Constant
α_m	Constant coefficient
β_m	Constant coefficient
Δ	Area of element
ε_1	Coefficient of horizontal eddy viscosity
ε_2	Coefficient of vertical eddy viscosity
η	Free-surface elevation

θ	Spherical coordinate
μ	Dynamic viscosity constant
ξ	Response to arbitrary tsunami
ρ	Mass density
$\rho(\omega)$	Phase angle
σ^2	Tidal variance
τ_b	Bottom stress
Φ	Velocity potential
Φ_A	Velocity potential in region A
Φ_B	Velocity potential in region B
Φ_I	Velocity potential of incident wave
Φ_S	Velocity potential of scattered wave
ω	Angular frequency
∇	Gradient operator

Abstract of Dissertation Presented to the Graduate Council of
The University of Florida in Partial Fulfillment of the Requirements
For the Degree of Doctor of Philosophy

TSUNAMI INTERACTION WITH COASTLINES AND ELEVATION PREDICTIONS

By

James Robert Houston

June 1978

Chairman: K. Millsaps
Cochairman: J. L. Hammack
Major Department: Engineering Science

The development is described of two numerical models that accurately simulate the propagation of tsunamis to nearshore regions and the interaction of tsunamis with coastlines. One of these models is a finite element model which uses a telescoping numerical grid to cover a section of the Pacific Ocean, including all eight islands of the Hawaiian Islands. The second model is a finite difference scheme that uses four rectilinear grids to cover most of the west coast of the continental United States. The finite element model solves linear and dissipationless long-wave equations. Such equations govern nearshore propagation in the Hawaiian Islands since the short continental shelf of the islands limits the time available for nonlinearities and dissipation to cause significant effects. The finite difference model solves nonlinear long-wave equations that include bottom stress terms which are important for the long continental shelf of the west

coast of the United States. Both models are verified by hindcasting actual historical tsunamis and comparing the numerical model calculations with tide-gage recordings. A frequency of occurrence analysis of tsunami elevations at the shoreline in the Hawaiian Islands is described. This analysis is based upon local historical data with the finite element model used to interpolate between historical data recorded during the period of accurate survey measurements since 1946. Historical data recorded at Hilo, Hawaii, and dating to 1837 is used in conjuction with data recorded since 1946 in Hilo and throughout the Hawaiian Islands to reconstruct elevations at locations in the islands lacking data prior to 1946. Frequency of occurrence curves are determined for the entire coastline of the Hawaiian Islands using these reconstructed elevations. Since most of the west coast of the United States lacks local data of tsunami activity, a frequency of occurrence analysis of tsunami elevations is based upon historical data of tsunami occurrence in tsunamigenic regions in addition to numerical model calculations. A generation and deep-ocean propagation numerical model is used to propagate tsunamis with varying intensities from locations throughout the Aleutian-Alaskan and Peru-Chile regions to a water depth of 500 meters off the west coast. The nearshore finite difference model propagates these tsunamis from the 500 meter depth to shore. The frequency of occurrence of combined tsunami and astronomical tide elevations is determined by an analysis involving the numerical superposition of tsunamis and local tides.

CHAPTER I

INTRODUCTION

Tsunamis

Of all water waves that occur in nature, one of the most destructive is the tsunami. The term "tsunami," originating from the Japanese words "tsu" (harbor) and "nami" (wave), is used to describe sea waves of seismic origin. Tectonic earthquakes, i.e., earthquakes that cause a deformation of the sea bed, appear to be the principal seismic mechanism responsible for the generation of tsunamis. Coastal and submarine landslides and volcanic eruptions also have triggered tsunamis.

Tsunamis are principally generated by undersea earthquakes of the dip-slip type with magnitudes greater than 6.5 on the Richter scale and focal depths less than 50 kilometers. They are very long period waves (5 minutes to several hours) of low height (a few feet or less) when transversing water of oceanic depth. Consequently, they are not discernible in the deep ocean and go unnoticed by ships. Tsunamis travel at the shallow-water wave celerity equal to the square root of the acceleration due to gravity times water depth even in the deepest oceans because of their very long wavelengths. This speed of propagation can be in excess of 500 miles per hour in the deep ocean.

When tsunamis approach a coastal region where the water depth decreases rapidly, wave refraction, shoaling, and bay or harbor resonance may result in significantly increased wave heights. The great

period and wavelength of tsunamis preclude their dissipating energy as a breaking surf; instead, they are apt to appear as rapidly rising water levels and only occasionally as bores.

Over 500 tsunamis have been reported within recorded history. Virtually all of these tsunamis have occurred in the Pacific Basin. This is because most tsunamis are associated with earthquakes, and most seismic activity beneath the oceans is concentrated in the narrow fault zones adjacent to the great oceanic trench systems that are predominantly confined to the Pacific Ocean.

The loss of life and destruction of property due to tsunamis have been immense. The Great Hoei Tokaido-Nanhaido tsunami of Japan killed 30,000 people in 1707. In 1868, the Great Peru tsunami caused 25,000 deaths and carried the frigate U.S.S. Waterlee 1,300 feet inland. The Great Meiji Sanriku tsunami of 1896 killed 27,122 persons in Japan and washed away over 10,000 houses.

In recent times, three tsunamis have caused major destruction in areas of the United States. The Great Aleutian tsunami of 1946 killed 173 persons in Hawaii, where runup heights as great as 55 feet were recorded. The 1960 Chilean tsunami killed 330 people in Chile, 61 in Hawaii, and 199 in distant Japan. The most recent major tsunami to affect the United States, the 1964 Alaskan tsunami, killed 107 people in Alaska, 4 in Oregon, and 11 in Crescent City, California, and caused over 100 million dollars in damage on the west coast of North America.

Objective and Scope of Study

The objective of the present study is to determine tsunami elevation frequencies of occurrence at the shoreline for the Hawaiian Islands and the west coast of the continental United States. Such elevation predictions are required by the Pacific Ocean Division of the U. S. Corps of Engineers for use in tsunami flood hazard evaluations for floodplain management and the Federal Insurance Administration of the Department of Housing and Urban Development for flood insurance rate calculations.

The current trend of general population migration to coastal regions and the growth of the tourist industry makes it essential to know possible tsunami inundation levels even for coastal regions that are currently undeveloped. There are only a few isolated locations in the United States that have sufficient local historical data of tsunami activity to allow accurate predictions solely based upon historical data. This lack of historical data of tsunami activity on most of the coastline of the United States makes it necessary to use numerical models in addition to existing historical data to predict tsunami elevation frequency of occurrence. However, numerical models have not been successfully applied in the past to the simulation of actual tsunami nearshore propagation and interaction with coastlines. Therefore, two numerical models are developed in the present study to accurately simulate tsunami nearshore activity. Calculations of these deterministic numerical models are combined with probabilistic analyses based upon historical data to predict frequencies of occurrence of tsunami elevations for the Hawaiian Islands and the west coast of the United States.

CHAPTER II

TSUNAMI INTERACTION WITH THE HAWAIIAN ISLANDS

Introduction

Early studies of tsunami interaction with islands involved analytic investigations of the scattering of monochromatic plane waves by a single island of simple geometric shape. Omer and Hall (1949) determined the theoretical diffraction pattern for long-wave scattering by a circular cylinder in water of constant depth by adopting results from acoustic theory. They found qualitative agreement between this diffraction pattern and smoothed runup heights observed for the 1946 tsunami on the island of Kauai in the Hawaiian Islands. Hom-ma (1950) determined the diffraction pattern for long wave scattering off a circular cylinder surrounded by a parabolic bathymetry that extended to a prescribed distance offshore, beyond which the depth was constant.

Hydraulic models have been used to study tsunami interaction with single islands that are realistically shaped and surrounded by variable bathymetry. Van Dorn (1970) studied tsunami interaction with Wake Island using a 1:57000 undistorted scale model. Jordaan and Adams (1968) studied tsunami interaction with the island of Oahu in the Hawaiian Islands using a 1:20000 undistorted scale model. They found poor agreement between historical measurements of tsunami runup and the hydraulic model data. Scale effects (e.g. viscous effects) and the effects of the arbitrary boundaries that confine the model are

problems that are inherent in hydraulic modeling of tsunamis. The small heights of tsunamis relative to deep ocean depths is also difficult to simulate. Jordaan and Adams (1968) modeled waves to a vertical scale of 1:2000; thus, the waves had heights ten times the normal proportion. Even with this distortion, waves typically had heights in the model of only 0.3 millimeters.

Vastano and Reid (1966) studied the problem of the response of a single island to monochromatic plane waves of tsunami period using a finite difference numerical model. A transformation of coordinates allowed a mapping of the island shore as a circle in the image plane. The finite difference solution employed a grid which allowed greater resolution in the vicinity of the island than in the deep ocean.

Vastano and Bernard (1973) extended the techniques developed by Vastano and Reid (1966) to multiple-island systems. However, the transformation of coordinates technique allows high resolution only in the vicinity of one island of a multiple-island system. Thus, for the three-island system of Kauai, Oahu, and Niihau in the Hawaiian Islands, the two islands of Oahu and Niihau had to be represented by cylinders with vertical walls whose cross sections were truncated wedges. Kauai was represented by a circular cylinder with the surrounding bathymetry increasing linearly in depth with distance radially from the island until a constant depth was attained. A single Gaussian-shaped plane wave was used as input to the model. No comparisons were made with historical tsunami data for the three islands.

Hwang and Divoky (1975) presented a simulation of the 1964 tsunami at Hilo, Hawaii, using a finite difference numerical model. The 1964 Alaskan tsunami was generated and propagated across the deep ocean using

a finite difference numerical model employing a coarse grid. The Hawaiian Islands were too small to be represented by this numerical grid. A waveform was calculated at a point in water 5000 meters deep that was approximately 200 kilometers from where Hilo, Hawaii, would have been if the Hawaiian Islands could have been modeled. This waveform was used as input to a finite difference grid with fine grid cells that covered an area approximately 22 kilometers by 67 kilometers in the immediate vicinity of Hilo. The water depth along the input boundary of the fine grid varied from approximately 250 meters to 1500 meters. Hwang's approach neglected the influence of the Hawaiian Islands and of the varying bathymetry and depth changes between the deep ocean point and the fine grid input boundary on the tsunami arriving in Hilo. The numerical model calculations for the 1964 tsunami were in poor agreement with the Hilo tide gage recording of this tsunami.

A finite difference model employing a grid covering the eight major islands of the Hawaiian Island chain was used by Bernard and Vastano (1977) to study the interaction of a plane Gaussian pulse with the Hawaiian Islands. The square grid cells were 5.5 kilometers on a side and close to the minimum feasible (because of computer time and cost limitations) size for a rectangular cell finite difference grid covering the major islands of Hawaii. Yet historical data indicate that significant variations of tsunami elevations occur over distances much less than 5.5 kilometers. The islands of Hawaii are relatively small and very poorly represented by a 5.5 kilometer grid. For example, Oahu has a diameter of only approximately 30 kilometers and the land-water boundary of the island has characteristic direction changes

that occur over distances much less than 5.5 kilometers. The offshore bathymetery of the islands also varies rapidly, with depth changes of more than 1500 meters frequently occurring in distances of 5.5 kilometers. Furthermore, if a resolution of eight grid cells per tsunami wavelength is maintained for tsunami periods as low as 15 minutes, a 5.5 kilometer grid cannot be used to propagate waves into depths less than approximately 150 meters. The processes that cause significant wave modifications and subsequent rapid variations of elevations along the coastline (that are known from historical observations to occur during tsunami activity in the Hawaiian Islands) probably occur within this region extending from water at a depth of 150 meters to the shoreline.

In the present study, a finite element numerical model is used to propagate tsunamis from the deep ocean to the shoreline of the Hawaiian Islands. Since finite element techniques allow dramatic changes in element sizes and shapes, this model has great advantages relative to finite difference numerical models in accurately representing land shapes, ocean bathymetry, and tsunami waveforms. Element size can be large in deep water where bathymetric variations are gradual and wave lengths are long. As a wave enters shallow water its length decreases and the elements of the grid can be telescoped to smaller sizes with no accompanying loss of resolution.

Governing Equations

Typical tsunamis have lengths much greater than the water depths over which they propagate; for such waves, fluid motions are

approximately two-dimensional, i.e., vertical fluid velocities and accelerations are small in comparison with horizontal velocities and accelerations, respectively.

Consider a small element of fluid as shown in Figure 1. The rate of increase of volume of the element is given by

$$\frac{\partial}{\partial t}\{(\eta+h)\ dxdy\} = \frac{\partial \eta}{\partial t}\ dxdy \tag{2.1}$$

where,

η = a free-surface elevation,

h = the water depth,

t = time,

and (x,y) are Cartesian coordinates.

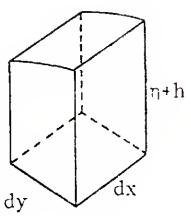

Figure 1. Element of Fluid

In Equation (2.1), it is assumed that $h=h(x,y)$, i.e. h has no time dependence. The net rate of volume flux is given in difference form by

$$\begin{aligned}
&\{u(\eta+h)\}_{x+dx}\,dy - \{u(\eta+h)\}_x dy \\
&+ \{v(\eta+h)\}_{y+dy}\,dx - \{v(\eta+h)\}_y dx \\
&= dxdy\ \{\frac{\partial}{\partial x}\,u(\eta+h) + \frac{\partial}{\partial y}\,v(\eta+h)\} + O(dx^2dy^2) \\
&= dxdy\ \nabla \cdot \vec{q}(\eta+h)
\end{aligned} \tag{2.2}$$

where u,v are horizontal velocity components, w is the vertical velocity component ($w=0$ here), and $\vec{q} = (u,v,w)$ is a velocity vector (a Taylor expansion is used in Equation (2.2) and terms of order dx^2dy^2 have been dropped). Equating the rate of increase of volume to the rate of volume flux yields the following continuity equation:

$$\frac{\partial \eta}{\partial t} + \nabla \cdot \vec{q}(\eta+h) = 0 \tag{2.3}$$

The governing momentum equation for incompressible and constant viscosity fluid flow is the Navier-Stokes equation in the form

$$\rho \frac{\partial \vec{q}}{\partial t} + \vec{q} \cdot \nabla \vec{q} = \rho \vec{F} - \nabla p + \mu \nabla^2 \vec{q} \tag{2.4}$$

where

p = the fluid pressure,

ρ = the mass density,

μ = the dynamic viscosity constant,

$\vec{F}$ = an external force vector.

Since vertical fluid velocities and accelerations are small and assuming that gravity is the only external force and the fluid is inviscid so that the last term of Equation (2.4) can be dropped, Equation (2.4) becomes in component form

$$\frac{\partial u}{\partial t} + u \frac{\partial u}{\partial x} + v \frac{\partial u}{\partial y} = - \frac{1}{\rho} \frac{\partial p}{\partial x} \tag{2.5}$$

$$\frac{\partial v}{\partial t} + u \frac{\partial v}{\partial x} + v \frac{\partial v}{\partial y} = - \frac{1}{\rho} \frac{\partial p}{\partial y} \tag{2.6}$$

$$0 = - \frac{1}{\rho} \frac{\partial p}{\partial z} - g \tag{2.7}$$

When integrated, Equation (2.7) yields (with atmospheric pressure equal to zero)

$$p = -\rho g(\bar{z}-\eta) \tag{2.8}$$

i.e., the pressure is hydrostatic, and

$$\nabla p = \rho g \nabla \eta \tag{2.9}$$

Equations (2.5) and (2.6) can be recombined to yield

$$\frac{\partial \vec{q}}{\partial t} + (\vec{q} \cdot \nabla)\vec{q} = -g\nabla\eta \tag{2.10}$$

Since along most of the path of propagation of a tsunami the wave amplitude is much less than the water depth, Equation (2.3) can be approximated as

$$\frac{\partial \eta}{\partial t} + \nabla \cdot (h\vec{q}) = 0 \tag{2.11}$$

It can also be shown that the second term in Equation (2.10) is generally less than the other terms by a factor of the order of η/h. Therefore, for η/h small, Equation (2.10) is approximated by

$$\frac{\partial \vec{q}}{\partial t} = -g\nabla\eta \tag{2.12}$$

Taking a time derivative of Equation (2.12) and substituting Equation (2.11) into the right-hand side of the subsequent equation yields

$$\frac{\partial^2 \vec{q}}{dt^2} = g\nabla(\nabla \cdot (h\vec{q})) \tag{2.13}$$

Equation (2.13) is known as the linear long wave equation. It is a governing equation for small amplitude long waves in an inviscid and incompressible variable depth fluid and is valid when the assumptions made in its derivation remain valid.

Assuming that the fluid is irrotational $\vec{q}$ can be expressed as a gradient of a scalar function $\Phi(x,y,t)$, known as the

velocity potential, i.e,

$$\vec{q} = \nabla\Phi \tag{2.14}$$

Assuming all motions to be simple harmonic in time yields

$$\Phi(x,y,t) = \mathrm{Re}\,[\Phi(x,y)e^{-i\omega t}] \tag{2.15}$$

where Re [ ] indicates the real part of the braced quantity, and ω is the frequency of the motion. Substituting Equations (2.14) and (2.15) into (2.13) yields

$$\nabla \cdot (h\nabla\Phi) + \frac{\omega^2}{g}\Phi = 0 \tag{2.16}$$

Equation (2.16) is the well known generalized Helmholtz equation. The wave amplitude η can be related to the velocity potential Φ by evaluating the Bernoulli equation at the free surface. The Bernoulli equation is given by

$$\frac{\partial\Phi}{\partial t} = \frac{P}{\rho} - gz + \frac{1}{2}|\nabla\Phi|^2 = 0 \ , \tag{2.17}$$

however; the last term in Equation (2.17) is generally smaller than the others by a factor of the order of η/h and can be neglected. Also, taking $p=0$ at the free surface where $z=\eta$, Bernoulli's equation becomes to the same order of approximation as Equation (2.16)

$$\eta = -\frac{1}{g}\frac{\partial\Phi}{\partial t}\Big|_{z\,=\,0} \tag{2.18}$$

Several assumptions are made in the derivation of Equations (2.16) and (2.18) and the adequacy of these assumptions for the particular problem of tsunami interaction with the Hawaiian Islands must be considered. An important factor in this consideration is the fact that the continental shelf of the Hawaiian Islands is exceptionally short. Thus, during most of the time of tsunami propagation, fluid velocities are much less than wave propagation velocities since wave amplitudes

are much less than water depths and bottom stress forces as well as nonlinearities have little time to cause significant effects.

Ursell (1953) and Hammack (1972) have shown that nonlinear effects grow with time. However, for a typical large tsunami, such as the 1964 Alaskan tsunami; Hammack and Segur (1977) have shown that neither nonlinearity nor frequency dispersion have any significant effect on the lead wave as it propagates across the ocean. In addition, when the lead wave reaches a continental shelf a certain time must pass before nonlinearity or frequency dispersion become significant. For a typical large tsunami, Hammack and Segur (1977) show that linear and nondispersive theory holds for the lead wave over a distance of approximately $\frac{2h^2}{a}$ (a is a wave amplitude). Taking the average depth of the region from the edge of the continental shelf (600 foot depth) to shore as 300 feet and the average amplitude as 3 feet (the amplitude becomes large only near shore) yields $\frac{2h^2}{a}$ = 12 miles. This distance is much greater than the length of the continental shelf of the Hawaiian Islands (usually less than 1 mile). Since the lead wave is followed by waves which have been reflected by land areas in the generation region, linear and nondispersive theory should be adequate, at least for the major waves of a tsunami.

Finite Element Model

Figure 2 shows the problem of tsunami interaction with islands with the process divided into two domains. One domain (A) includes the islands and the surrounding variable depth region. The second domain (B) is a constant depth region extending to infinity. This constant

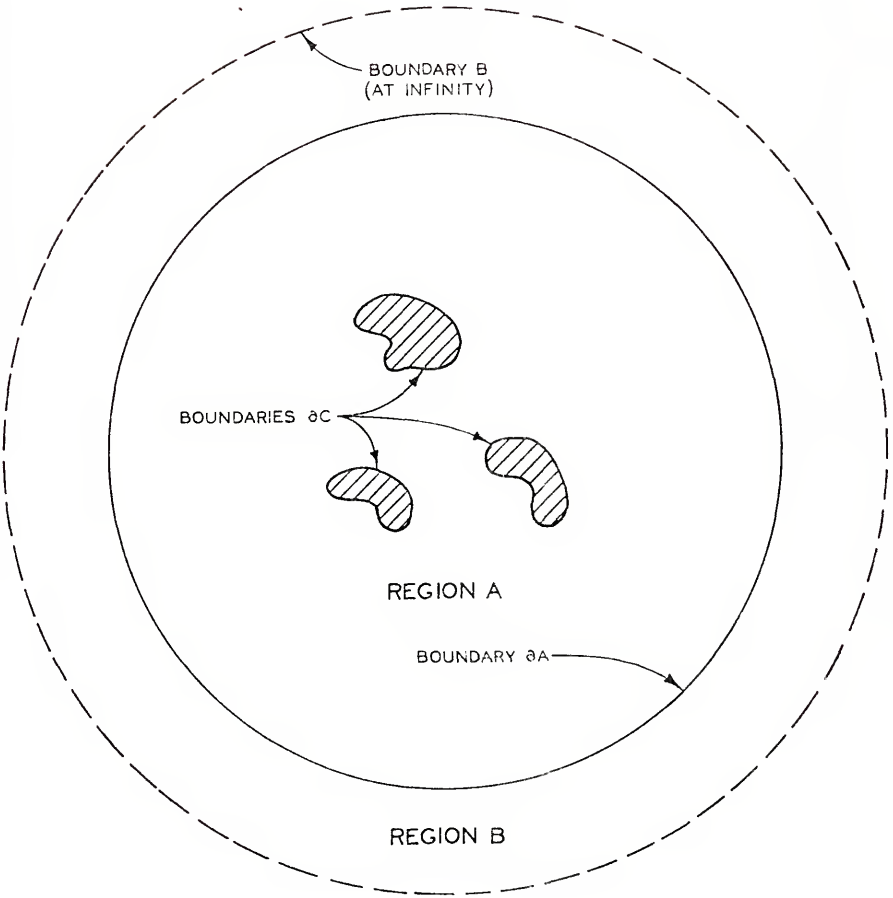

Figure 2. Regions of Computation.

depth region is realistic since the Pacific Ocean has a remarkably constant depth beyond the immediate region of the Hawaiian Islands. The boundary value problem expressed in terms of these domains becomes the following:

$$\nabla \cdot (h\nabla\Phi) + \frac{\omega^2}{g}\Phi = 0 \qquad \text{in Region A} \tag{2.19}$$

$$\nabla \cdot (\nabla\Phi) + \frac{\omega^2}{gh}\Phi = 0 \qquad \text{in Region B} \tag{2.20}$$

$$\Phi_A = \Phi_B \qquad \text{on } \partial A \tag{2.21}$$

$$\left(h\frac{\partial\Phi}{\partial n_A}\right)_A = \left(h\frac{\partial\Phi}{\partial n_A}\right)_B \qquad \text{on } \partial A \tag{2.22}$$

$$\frac{\partial\Phi}{\partial n} = 0 \qquad \text{on } \partial C = \partial C_1 + \partial C_2 \ldots . \partial C_j \tag{2.23}$$

$$\lim_{r \to \infty} (r)^{1/2} \left(\frac{\partial}{\partial r} - ik\right)\Phi_S = 0 \tag{2.24}$$

where

j = number of land masses,

r = a spherical coordinate,

k = the wave number,

Φ_S = the scattered wave velocity potential,

$i = (-1)^{1/2}$.

Equations (2.21) and (2.22) express the continuity of the velocity potential and its derivative along the boundary separating the two domains and Equation (2.23) expresses the impermeability of solid boundaries. Equation (2.24) is the Sommerfeld radiation condition that requires the scattered wave to be an outgoing wave at infinity.

A calculus of variations approach can be used to obtain an Euler-Lagrange formulation of boundary value problems. This variational formulation is based upon the principle that of all possible displace-

ment configurations a body can assume that satisfy compatibility and the constraints of kinematic boundary conditions, the configuration satisfying equilibrium makes the potential energy a minimum. The Euler-Lagrange formulation of boundary value problems has often been used in classical dynamics (Hamilton's principle of least action) and solid mechanics (structural, solid, and rock mechanics). Of course, it is not possible to obtain analytical solutions for many engineering problems. The finite element method is a numerical method first introduced by Turner et al. (1956) (although some of the underlying ideas were discussed by Courant (1943)) which has found wide application in solid mechanics for problems based upon an Euler-Lagrange formulation involving complex material properties or boundary conditions (see Zienkiewicz, 1971 and Desai and Abel, 1972). The finite element method is a discrete approximation procedure applicable whenever a variational principle can be formed. This method has a very short history in fluid mechanic applications despite advantages over conventional numerical schemes such as finite difference methods. The first application of the finite element method to fluid mechanic problems involved a study by Zienkiewicz and Cheung (1966) of seepage through porous media.

Chen and Mei (1974) studied the problem of the forced oscillation of a small basin protected by a breakwater and containing floating nuclear power plants by using the finite element method. They discretized a small constant depth region using approximately 250 triangular elements that were all about the same size and shape. Since small amplitude long waves were used as a forcing function, Equation (2.20) was the

governing equation (the water depth being constant in their application). In the present study an approach similar to that of Chen and Mei is used to solve the problem of tsunami interaction with islands in a variable depth region.

For the finite element method to be useful for tsunami problems, it is necessary to take advantage of two important properties of this algorithm. First, the finite element grid which discretizes a domain can have grid cells (elements) of arbitrary size and shape. Thus, the grid can telescope from a large cell size in one section of a variable depth domain to a very fine cell size in another. Secondly, if the form of the spatial variation of a physical parameter is known a priori, the finite element method can employ a very small number of elements in the discretization used to estimate the exact variation. For example, a single finite element can be used to solve the problem of the seiching of a lake for a constant depth rectangular lake if the basic form (unknown coefficients) of the solution is known. The finite element method degenerates into the well-known Rayleigh-Ritz variational method in this case. This property of the finite element method will be important in modeling the infinite region B shown in Figure 2.

The variational principle for the boundary value problem given by Equations (2.19) through (2.24) requires a certain functional $F(\Phi)$ to be stationary with respect to arbitrary first variation of Φ. The first variation of the functional $F(\Phi)$ for this problem is well-known and can be expressed as

$$\delta F(\Phi) = -\iint_A [\nabla \cdot (h\nabla\Phi) + \frac{\omega^2}{g}\Phi]\,\delta\Phi + \int_{\partial A} h(\Phi_B - \Phi_A)\frac{\partial \delta\Phi_B}{\partial n_A}$$

$$+\int_{\partial A}[(h\frac{\partial\Phi}{\partial n_A})_A - (h\frac{\partial\Phi}{\partial n_A})_B]\,\delta\Phi_A - \int_{\partial C} h\frac{\partial\Phi_A}{\partial n_A}\,\delta\Phi_A = 0 \qquad (2.25)$$

The functional can be derived from this expression for its first variation (Chen and Mei, 1974) and is

$$F(\Phi) = \iint_A \frac{1}{2}[h(\nabla\Phi)^2 - \frac{\omega^2}{g}\Phi^2] + \int_{\partial A}\frac{1}{2}h(\Phi_B - \Phi_I)\frac{\partial(\Phi_B - \Phi_I)}{\partial n_A}$$

$$-\int_{\partial A} h\Phi_A\frac{\partial(\Phi_B - \Phi_I)}{\partial n_A} - \int_{\partial A} h\Phi_A\frac{\partial\Phi_I}{\partial n_A}$$

$$+\int_{\partial A} h\Phi_I\frac{\partial(\Phi_B - \Phi_I)}{\partial n_A}\,, \qquad (2.26)$$

where Φ_I is the velocity potential of the incident waves (forcing function).

The finite element method (unlike the finite difference method) discretizes the domain itself rather than the governing equations. The region under consideration is partitioned into small regions known as finite elements and the assemblage of all such elements represents the original region. Instead of solving the problem for the entire body in one operation, the solutions are formulated for each constituent element and combined to obtain the solution for the original region. Thus, for example, the first term of Equation (2.26) is evaluated on the element level and the results for all elements are summed. This sum is equivalent to the original integral over the complete region A.

In order to evaluate the first term in Equation (2.26) on the element level, it is necessary to approximate the field variable Φ

within each element by a polynomial N, called a trial or interpolation function, in the coordinates x and y.

For each element

$$\Phi = \{N\}\{\phi\} \tag{2.27}$$

where

$$\{\phi\} = \begin{bmatrix} \phi_i \\ \phi_j \\ \phi_k \end{bmatrix} \tag{2.28}$$

is a column vector with ϕ_i, ϕ_j, ϕ_k the unknown values of the field variable at the nodal points (vertices) of a triangular element and

$$\{N\} = [N_i, N_j, N_k] \tag{2.29}$$

is a row vector with

$$N_i = (a_i + b_i x + c_i y)/2\Delta \quad (i=1,2,3) \tag{2.30}$$

$$a_i = x_k y_j - x_j y_k \tag{2.31}$$

$$b_i = y_k - y_j \tag{2.32}$$

$$c_i = x_j - x_k \tag{2.33}$$

and Δ is the area of the element. The coordinates of the nodal point i are (x_i, y_i) and the N_j and N_k are similarly expressed by the cyclical permutation of i, j, and k.

A linear interpolation function can be used for tsunamis propagating within region A since elements within this region will always be much smaller than local wavelengths (long waves are adequately represented as linear variations over such short distances). The convergence of the solution is assured as the elements are made infinitesimal (Strang and Fix, 1973). Since each element has its own polynomial

expansion independent of all other elements, the treatment of the entire domain is systematically handled by summing the contributions from each element.

The expression $\Phi_B - \Phi_I$ in Equation (2.26) is the scattered wave velocity potential Φ_S. Since region B has a constant depth, Φ_S can be solved analytically. The governing equation for this case is the Helmholtz equation (Equation (2.20)). The boundary condition at infinity requires the scattered wave obey the Sommerfeld radiation condition given by Equation (2.24). The well-known solution to this boundary value problem is as follows:

$$\Phi_S = \sum_{m=0}^{\infty} H_m(kr) \, (\alpha_m \cos m\theta + \beta_m \sin m\theta) \tag{2.34}$$

where

H_m are Hankel functions of the first kind of order m,

α_m and β_m are constant coefficients,

and θ is a spherical coordinate.

In the finite element formulation, the infinite region B can be considered to be a single element with the interpolation function given by Equation (2.34). Thus, within region A the interpolation functions are linear, but within region B the interpolation function is an infinite series involving unknown coefficients. The terms in Equation (2.34) are oscillatory but have a monotonically decreasing modulation; hence, the series can be truncated after a finite number of terms depending upon the desired accuracy (see next section).

The required stationarity of the functional $F(\Phi)$ with respect to arbitrary variations of Φ at each nodal point yields a set of linear algebraic equations when expressed on the element level that can be solved using matrix methods. For each specified incident wave period,

the velocity potential ϕ can be determined at all nodal points. The linearized dynamic free surface boundary condition (Equation (2.18)) can then be used to calculate the surface elevation η.

The set of linear algebraic equations evolving from the element level can be written in the simple matrix form

$$[K]\ \{\psi\} = \{Q\} \tag{2.35}$$

where $[K]$ is the large coefficient matrix, $\{\psi\}$ is a column vector representing a combination of nodal unknowns for the velocity potential and the coefficient unknowns from the single element covering region B, and $\{Q\}$ is the total load column vector related to the forcing function. In the finite element solution of structural mechanics problems, one obtains a similar equilibrium relation with $[K]$ being a stiffness matrix, $\{\psi\}$ a nodal displacement vector, and $\{Q\}$ a nodal force vector (Desai and Abel, 1972). The coefficient matrix $[K]$ is symmetric, banded, and complex (complex notation was used to represent waveforms, e.g., the Hankel functions are complex). For the case of tsunami interaction with the Hawaiian Islands, $[K]$ will be exceptionally large and sparse (many zero terms). Of course, only half of the banded part of the matrix alone needs to be manipulated in the solution process. The banded part of the matrix $[K]$ is solved using standard Gaussian elimination methods. The matrix solution used by Chen and Mei (1974) was modified in this study to take advantage of the sparseness of the matrix in order to reduce computational time. Also, the elimination method was modified so that calculations involved only small blocks of terms at a time with the remainder of the matrix kept in peripheral storage. This matrix partitioning was necessary for the finite element grid shown in the next

section since the banded part of the matrix had over 800,000 terms. Partitioning is possible because the symmetric coefficient matrix is positive definite; hence, a solution is possible by elimination methods without pivoting. Without pivoting, elimination performed using one row, affects only the triangle of elements within the band below that row. Thus, only two triangular submatrices needed to be stored in computer memory at a given time.

Numerical Grid

The finite element grid covering the variable depth region A is shown in Figure 3. Elements of the grid telescope from large sizes in the deep ocean to triangles with areas as small as 0.5 square kilometers in shallow coastal waters. The grid covers an area of approximately 450,000 square kilometers. In general, finite element techniques allow elements to be any arbitrary shape (e.g. quadrilateral) provided that the ratio of the lengths of the shortest and longest sides of an element is not extreme. Triangular shapes were used for convenience in the present study.

The geometric shapes of the eight islands comprising the Hawaiian Island chain and the rapid bathymetric variations surrounding the islands are modeled very precisely by the finite element grid of Figure 3. Also, the number of node points along the shorelines of the islands is very dense. Since wave heights are calculated at node points by the finite element model, the model can adequately represent the rapid wave-height variations along coastlines that are known to occur during tsunami activity in the Hawaiian Islands.

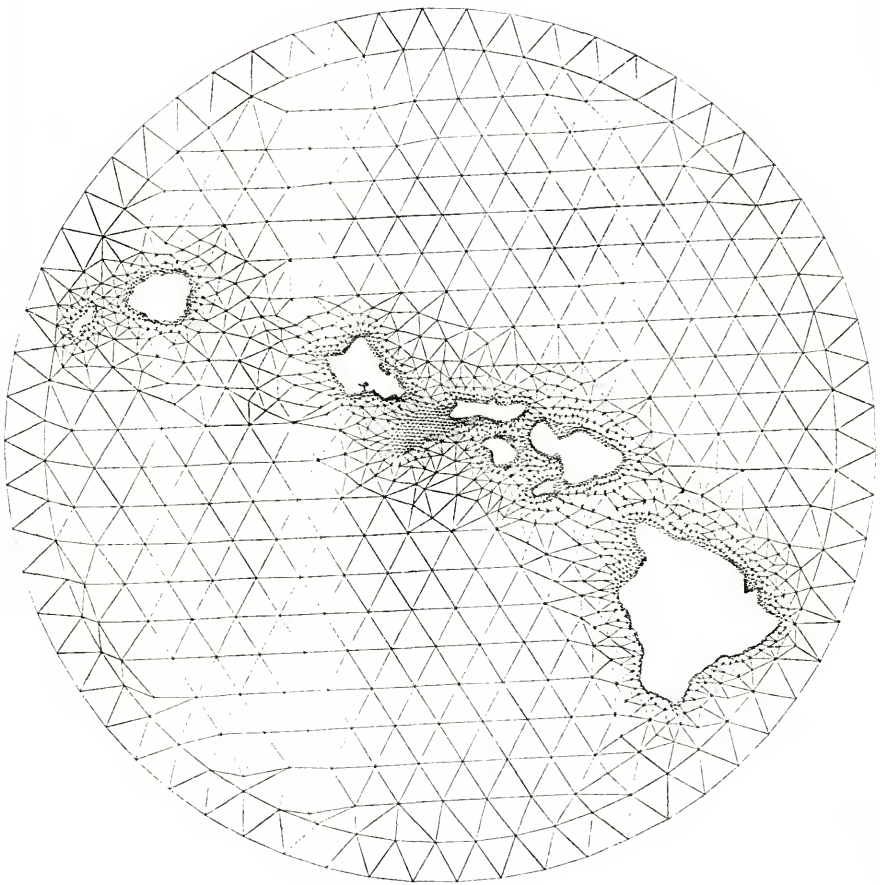

Figure 3. Finite Element Grid.

The finite element grid was drawn by hand with the element sizes dictated by the local water depth. The lengths of element sides were allowed to be no greater than one-eighth of the local wavelength for the shortest period waves considered. Such a cell size results in a wave resolution error of no more than one percent (Mei 1978). There are computer programs (Cole and Riech, 1976) that generate finite element grids and number the nodes to minimize bandwidths; however, such programs only can be applied to fairly homogeneous domains. The rapid depth variations in region A require a rapidly telescoping grid that is too complicated for automatic grid generation techniques.

Each node of the finite element grid must be numbered and this numbering is extremely important since it determines the bandwidth of the large coefficient matrix discussed in the last section. The bandwidth of this matrix is controlled by the largest difference (among all elements) in the nodal numbers between two nodes of the same element. The computational time of the numerical model is proportional to the cube of the bandwidth of the coefficient matrix.

For a simple region covered by homogeneous elements, the bandwidth is minimized by numbering nodal points in cyclic sequence following a spiraling pattern where one spiral is shielded by the following spiral from a third spiral. The grid pictured in Figure 3, however, is so large and complicated that considerable judgement and effort is involved in determining a numbering pattern that minimizes the bandwidth, thus resulting in reasonable computational times for the numerical model.

The numerical model also requires the spatial coordinates of all node points and information concerning how the elements are connected

relative to each other (connectiveness). The coordinates were determined using an electronic digitizer and a simple computer program developed to relate the internal coordinate system of the digitizer to a prototype coordinate system through coordinate rotation and scaling. The elements are numbered in an arbitrary fashion and then connectiveness information assembled for the numerical model by listing the three nodes of each element.

The nodal numbering, digitizing, and connectiveness assembly necessarily introduce errors. For example, the connectiveness assembly involves determining over 17,000 numbers and placing them on computer cards. Many connectiveness mistakes do not result in error conditions which terminate the numerical model's computations. Instead, incorrect answers are produced by the model. To eliminate all errors in the input data, computer plotting programs were developed to draw the grid and number nodes and elements based upon the connectiveness and node coordinate information used as input to the numerical model. Such plots make errors readily apparent.

The number of terms retained in the truncation of Equation (2.34) was determined by trial and error. The final number of terms was such that addition of further terms produced negligible effects. It was found that this occurs for terms approximately 10^{-5} times smaller than the initial terms.

The computational time requirements of the finite element model for the grid shown in Figure 3 are very modest, making it economically feasible to determine the interaction of arbitrary tsunamis with the Hawaiian Islands (discussed in next section). The reason that the

computationtal time required by the finite element model is reasonably small is that the grid uses small elements only in areas where they are necessary. The grid of Figure 3 has approximately 2500 points, whereas the finite difference grid of Bernard and Vastano (1977) had 26,000 grid points. Even so, some of the elements of Figure 3 are as much as sixty times smaller than the finite difference grid cells used by Bernard and Vastano.

Model Verification

The finite element model is verified in the present study by comparing numerical simulations of the 1960 Chilean and 1964 Alaskan tsunamis with tide gage recordings of these tsunamis in the Hawaiian Islands. These two tsunamis are the only major tsunamis for which reliable information exists concerning characteristics of the ground uplift which generated the waves (much more information exists for the Alaskan source).

A deep ocean recording of a tsunami near the Hawaiian Islands has never been made. Therefore, prototype wave records in the deep ocean of the 1960 Chilean and 1964 Alaskan tsunamis are not available for use as input to verify the finite element model. However, a finite difference numerical model which solves the linear long wave equations employing a spherical coordinate grid has been developed (Hwang et al., 1972), and used in several studies (Houston and Garcia, 1974; Houston and Garcia, 1975; and Houston et al., 1975b) to generate tsunamis and propagate them across the deep ocean. This deep ocean numerical model

is used in this study to determine deep ocean waveforms of the 1960 and 1964 tsunamis that were needed to verify the finite element model.

The deep-ocean numerical model simulates the uplift deformation of the ocean water surface caused by the permanent vertical displacement of the ocean bottom during an earthquake and the subsequent propagation of the resulting tsunami across the deep ocean. The permanent deformation (permanent in the sense that the time scale associated with it is much longer than the period of the tsunami) and not the transient movements within the time-history of the ground motion is considered to be the important parameter governing far-field wave characteristics. Transient movements occur for a period of the order of tens of seconds, whereas, tsunami wave periods are of the order of tens of minutes. Experimental investigations of tsunami generation by Hammack (1972) show that the transient ground movements do not influence far-field characteristics of resulting tsunamis for spatially large ground displacements occurring over a short period of time.

Hwang et al. (1972) verified the deep ocean model by simulating the 1964 Alaskan tsunami. The permanent ground deformation in the source region was taken from Plafker (1969) and a 1/4° by 1/6° grid was used for the simulation. Since this grid was much too coarse to allow accurate modeling of shallow-water propagation, a comparison was made between the numerical model calculations and a gage recording of the 1964 tsunami at Wake Island where Van Dorn (1970) had a pressure transducer in relatively deep water (800 foot depth) some distance offshore. The amplitude and length of the first wave of this tsunami were shown to be in good agreement. (Actually, the grid used by Hwang et al.

(1972), did not extend as far as Wake Island. The deep ocean model propagated the tsunami to a point in the Pacific Ocean and then simple refraction techniques were used to estimate the change in the waveform during propagation from this point to Wake Island.)

The simulation of the 1960 and 1964 tsunamis performed in this study uses a 1/3° by 1/3° grid. Prior simulations of the 1964 tsunami using both a 1/4° by 1/6° grid and a 1/3° by 1/3° grid demonstrated negligible differences between use of the two grid spacings (Houston et al., 1975a). The permanent ground deformation used as input is also taken from Plafker (1969). The numerical grid was large enough to cover a substantial portion of the Pacific Ocean including Wake Island. The numerical model calculations at Wake Island were found to be similar to those presented by Hwang et al. (1972). Figure 4 shows a comparison of the numerical model calculations of this study and the Wake Island recording of the 1964 tsunami. The lack of agreement in the trailing wave region may be due to local effects (e.g. wave trapping by the Wake Island seamount) or reflections from the nearby transmission boundaries of the numerical grid (these boundaries are not perfectly transmitting).

Figures 5 and 6 show time-histories of the 1960 Chilean and 1964 Alaskan tsunamis in deep water near the Hawaiian Islands calculated using the deep ocean propagation model. The permanent ground deformation in the source region of the Chilean earthquake of 1960 is taken from Plafker and Savage (1970). Calculations for the Alaskan tsunami involve a grid with approximately 30,000 cells and the calculations for the Chilean tsunami a grid with approximately 90,000 cells.

The finite element numerical model is a time-harmonic solution of

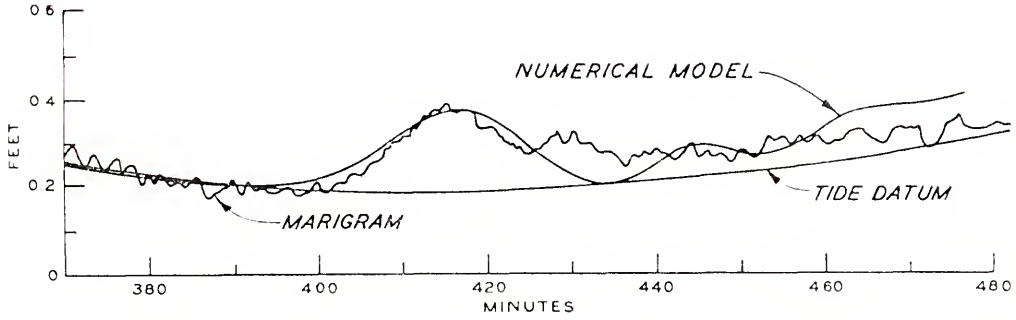

Figure 4. Comparison of Deep Ocean Numerical Model Calculations and Tide Gage Recording of the 1964 Tsunami at Wake Island.

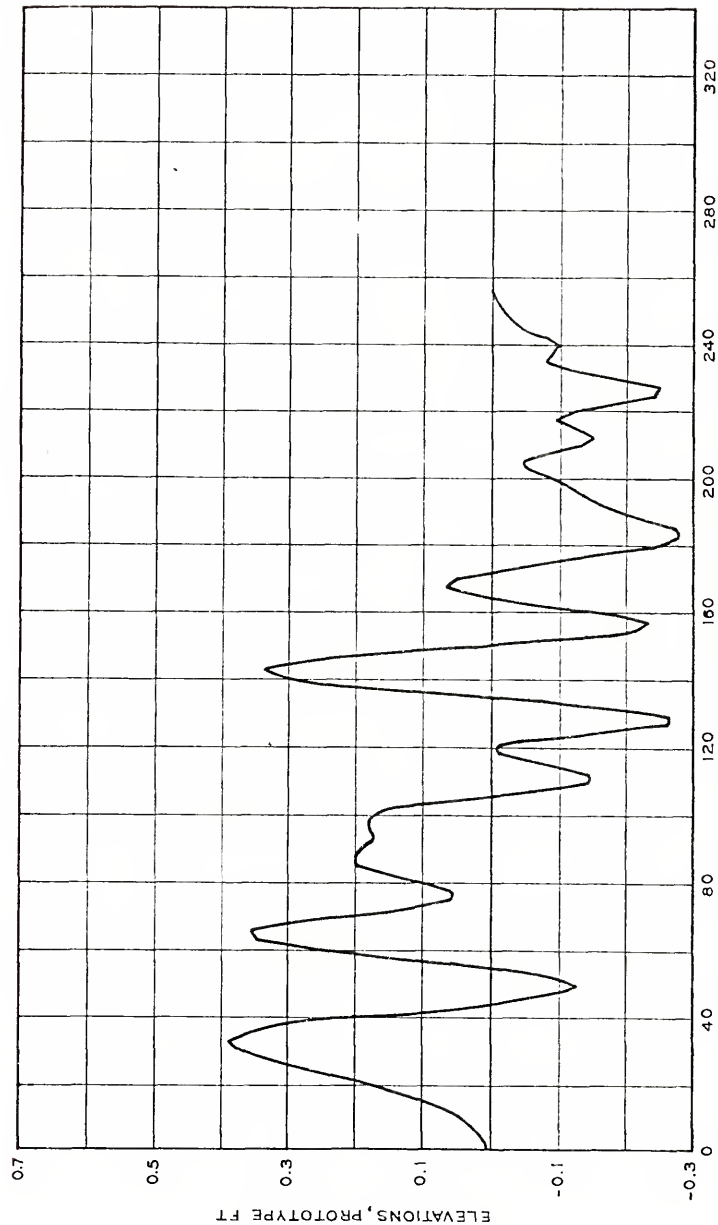

Figure 5. 1964 Alaskan Tsunami in Deep Water Near Hawaii as Calculated by the Finite Difference Numerical Model.

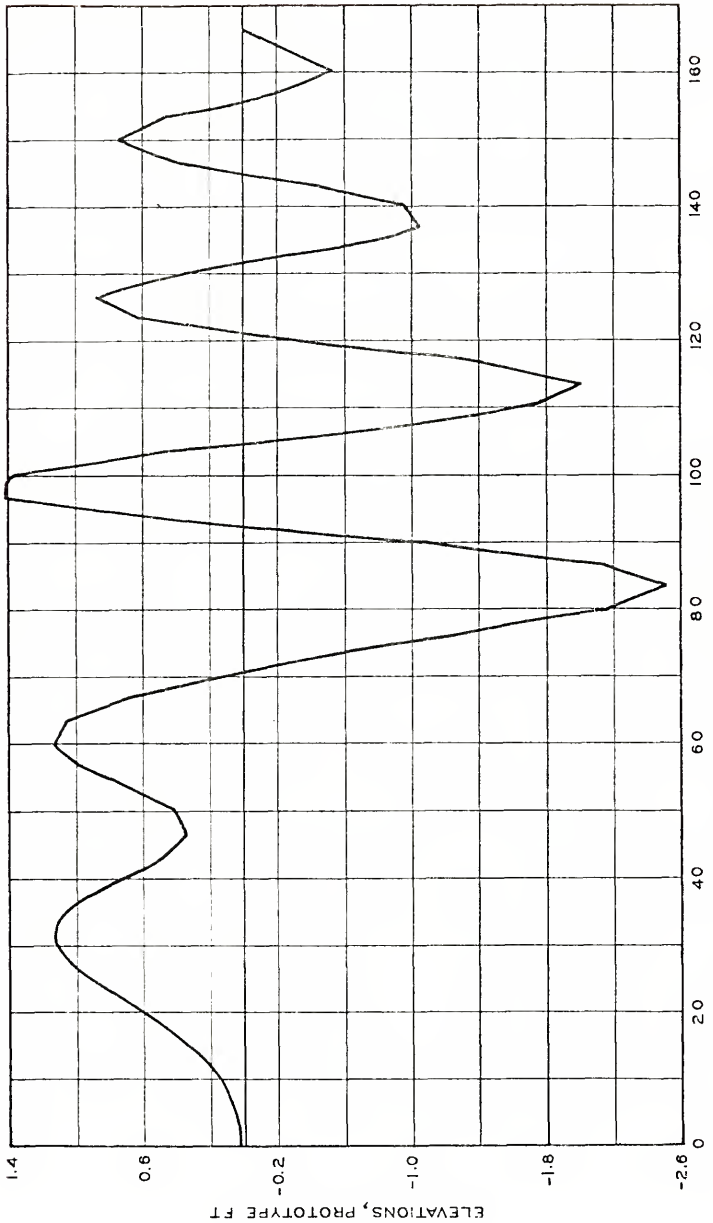

Figure 6. 1960 Chilean Tsunami in Deep Water near Hawaii as Calculated by the Finite Difference Numerical Model.

the boundary value problem. The response of a group of islands to an arbitrary tsunami can easily be determined within the framework of a linearized theory using the theory of superposition. For example, an arbitrary tsunami in the deep ocean can be Fourier decomposed as follows:

$$b_o(t) = \int_{\infty}^{\infty} b(\omega)\ e^{-i(\omega t+\rho(\omega))}\ d\omega \qquad (2.36)$$

where

b_o = incident wave amplitude

$b(\omega)$ = amplitude of frequency component ω

$\rho(\omega)$ = phase angle

If $\eta(x,y,\omega)$ is the response amplitude at any point (x,y) along the island coasts due to an incident plane wave of unit amplitude and frequency ω, then the response of the islands to the arbitrary tsunami time history $b_o(t)$ is given by

$$\xi(x,y,t) = \mathrm{Re}\left[\int_{\infty}^{\infty} b(\omega)\eta(x,y,\omega)\ e^{-i\{\omega t-\rho(\omega)\}}d\omega\right] \qquad (2.37)$$

Therefore, when $\eta(x,y,\omega)$ is known for all ω, the island response to an arbitrary tsunami can be calculated. Of course, it is not feasible to calculate the integrals of Equations (2.36) and (2.37) over all frequencies. Instead, the frequency range must be discretized and the integrals replaced by sums over a frequency range containing most of the energy of the tsunami.

Equation (2.36) involves a Fourier decomposition of a time series. This decomposition is accomplished for the time-histories of the 1960 Chilean and 1964 Alaskan tsunamis (Figures 5 and 6) using a least squares harmonic fitting procedure. The time-history of the Alaskan

tsunami in deep water was decomposed into 18 components with periods ranging from 14.5 minutes to the time length of the record (260 minutes). The variance of the residual (difference between the actual record and a recomposition of the 18 components) was approximately 0.2 percent of the variance of the record. Therefore, virtually all the energy of the wave record was contained in the 18 components. The time-history of the Chilean tsunami in deep water was decomposed into 11 components with periods ranging from 15.5 minutes to the time length of the record (170 minutes). The variance of the residual was less than 0.1 percent of the variance of the record. For both cases, the original time-history and a time-history constructed from a recomposition of the components were virtually indistinguishable.

Equations (2.36) and (2.37) take the following form when discretized:

$$b_o(t) = \sum_{n=1}^{m} b(\omega_n)\, e^{-i\{\omega_n t+\rho(\omega_n)\}} \tag{2.38}$$

$$\xi(x,y,t) = \mathrm{Re}\left[\sum_{n=1}^{m} b(\omega_n)\ \ \eta(x,y,\omega_n)\, e^{-i\{\omega_n t+\rho(\omega_n)\}}\right] \tag{2.39}$$

where

m = number of components,

ω_n = frequency of n^{th} component

The $b(\omega_n)$ term is determined by the least-squares harmonic fitting procedure and $\eta(x,y,\omega_n)$ is determined by the finite element numerical model for each frequency ω_n and at each location (x,y). Therefore, the time-history $\xi(x,y,t)$, which represents the response of location (x,y) to the deepwater tsunami time-history given by $b_o(t)$,

can be calculated for any location along the coastline of the Hawaiian Islands.

Figures 7, 8, and 9 present comparisons between tide gage recordings and numerical model calculations of the 1964 Alaskan tsunami at Kahului, Maui; Honolulu, Oahu; and Hilo, Hawaii, respectively. The largest waves recorded at each of these sites are shown. Waves arriving at later times are all much smaller than those shown. Whenever tide gage limits were encountered, the recordings were linearly extended (the tide gage locations are shown in Figure 10).

The wave records shown in these figures are in remarkable agreement, especially considering the fact that the ground displacement of the 1964 earthquake was not precisely known. Since the Hilo breakwater was not included in the numerical model, the numerical model calculations for Hilo are probably too large; however, this breakwater was undoubtedly highly permeable to the 1964 tsunami. The numerical results appear to be too large in Hilo by some constant factor, since the tide gage recording and the numerical model calculations have the same form with the first wave crest and trough having approximately the same amplitude and being proportionately smaller than the second crest.

Figure 11 shows a comparison between the tide gage recording of the 1960 Chilean tsunami at Honolulu and the numerical model calculations. Again the largest waves recorded are shown (the Honolulu gage was the only tide gage in the Hawaiian Islands not destroyed by the 1960 tsunami). The permanent ground motion of the 1960 earthquake is not known nearly as well as the ground motion for the 1964 earthquake.

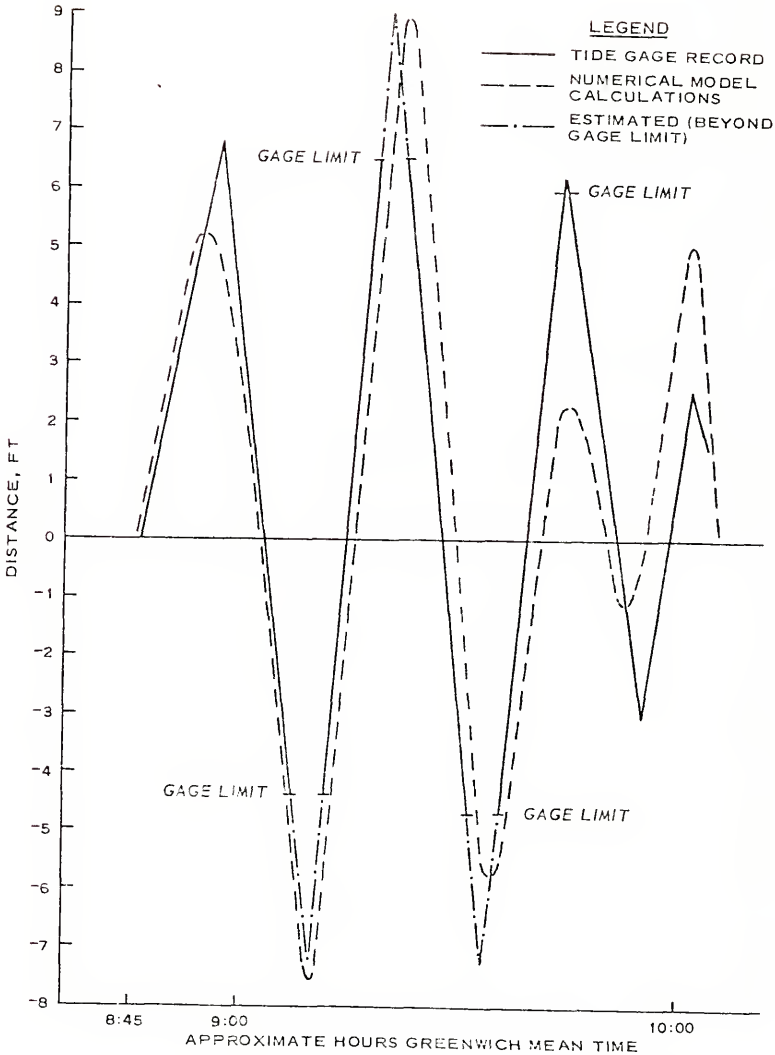

Figure 7. 1964 Tsunami from Alaska Recorded at Kahului, Maui.

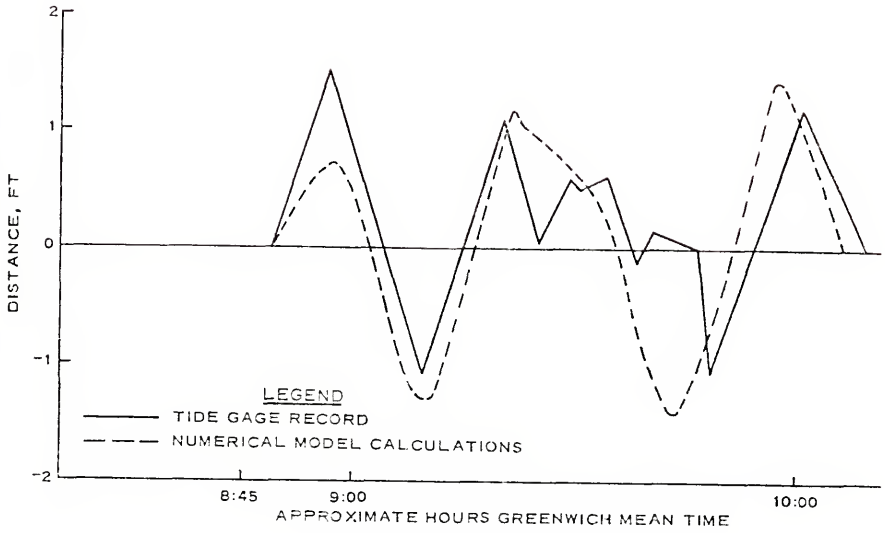

Figure 8. 1964 Tsunami from Alaska Recorded at Honolulu, Oahu.

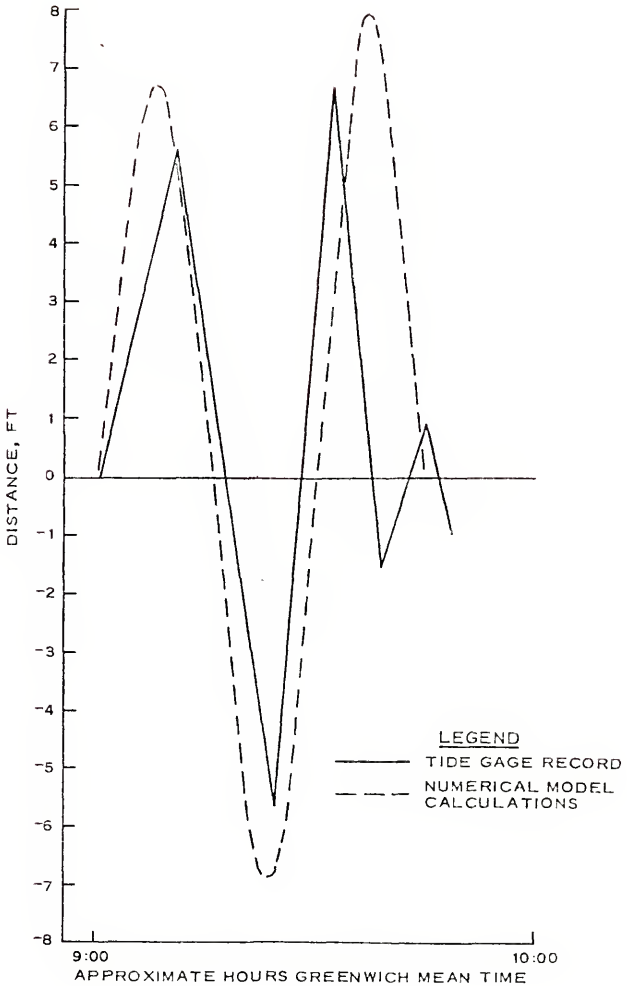

Figure 9. 1964 Tsunami from Alaska Recorded at Hilo, Hawaii.

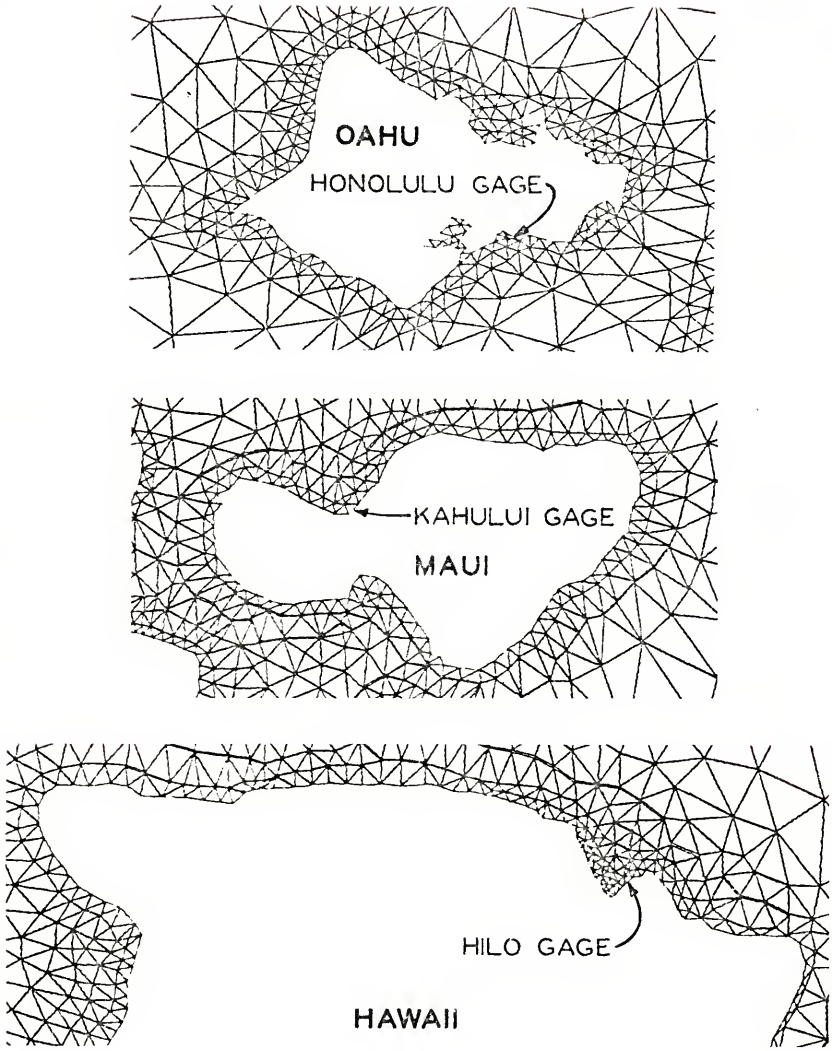

Figure 10. Gage Locations.

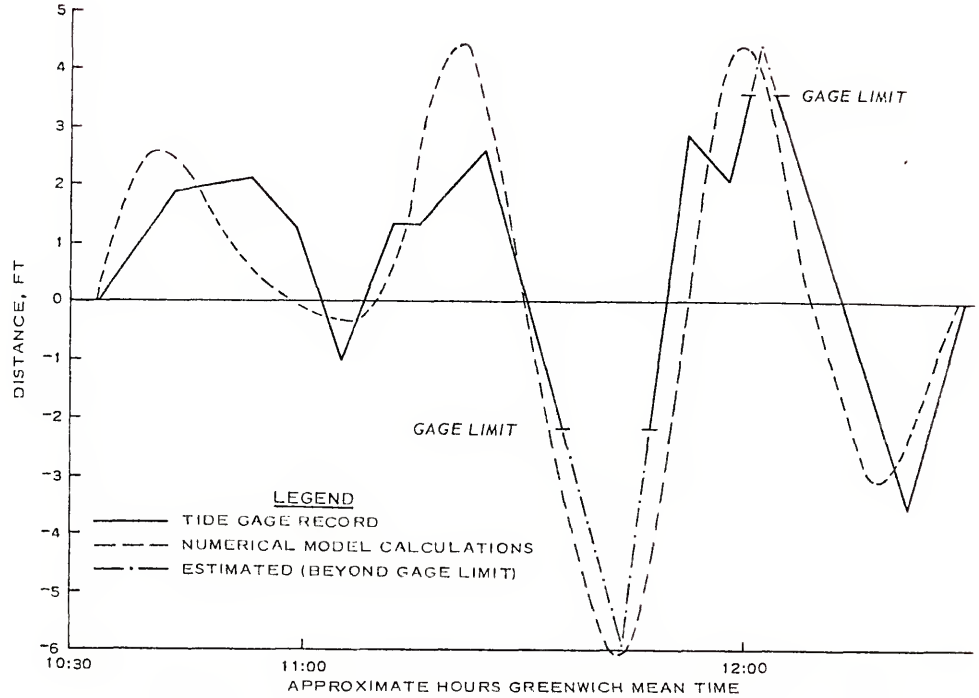

Figure 11. 1960 Tsunami from Chile Recorded at Honolulu, Oahu.

Hence, the agreement indicated in Figure 11 is quite good considering the uncertainty of the uplift in the source region.

Tide gages, of course, do not record tsunamis perfectly since they are nonlinear devices with responses which depend upon both the period and amplitude of the disturbances they measure. However, simple calculations based upon the paper of Noye (1970) show that the distortion is small for the tsunamis shown in Figures 7 through 9 and Figure 11.

Figure 12 shows the response amplitude as a function of wave period at the locations of tide gages in Kahului, Honolulu, and Hilo. The response versus wave period is greatly dependent upon the precise location of recording for bays such as Hilo. For example, the Hilo response (Figure 12) at the tide gage location shown in Figure 10 has a single large resonant peak at 28.9 minutes. This peak occurs at the fundamental period of oscillation of Hilo Bay and, consequently, all locations in the bay have a resonant peak at this incident wave period (the amplitude of the peak depends on location in the bay). Other locations in Hilo Bay also have significant peaks at lower periods. Loomis (1970) calculated a free oscillation fundamental period (node assumed at bay mouth) of 26.2 minutes for Hilo Bay using a finite difference grid spacing of approximately one-half a kilometer.

Bernard and Vastano (1977) show a contour map of a normalized energy parameter versus wave period and location around the island of Hawaii. The map shows Hilo displaying an energy peak from 10 to 16 minutes centered at approximately 12.5 minutes; no significant peak at 28.9 minutes is observed. The difference between Bernard and Vastano's calculations and the results presented in this paper is attributed to

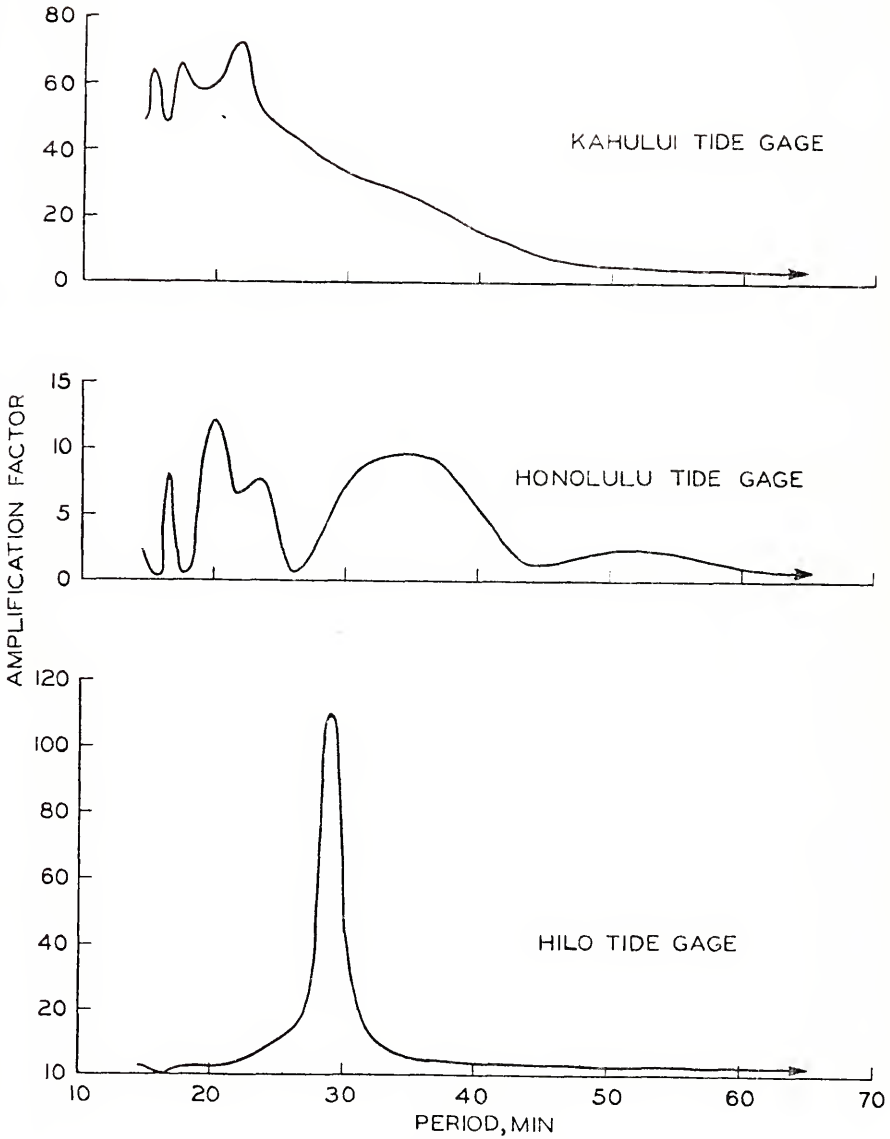

Figure 12. Amplification Factor Versus Wave Period.

the poor resolution of the spatial features of Hilo Bay by their finite difference grid spacing of 5.5 kilometers. Hilo Bay has the shape of a right triangle with sides that are approximately 9 kilometers and 13.5 kilometers long. The grid used by Bernard and Vastano represented Hilo Bay as a right triangle with sides that were 5.5 kilometers and 11 kilometers long; thus, the surface area of Hilo Bay was approximately one half its actual area. This distortion of the size of Hilo Bay and also, perhaps, the distortion of the bathymetry of the bay by the coarse grid accounts for the lower response periods for Hilo Bay presented by Bernard and Vastano.

The importance of accurately representing island shapes and offshore bathymetry and resolving tsunami wavelengths can be illustrated by considering a study by Adams (1975) that used the numerical model developed by Bernard and Vastano (1977) to interpolate between historical measurements of tsunami elevations produced by the 1946 Aleutian tsunami. A single Gaussian wave crest was used as input for the numerical model. If a resolution of four grid cells per crest wavelength is maintained, this numerical model cannot propagate waves into water with a depth less than about 500 feet. The main processes involved in the transformation of the form of a tsunami probably occur in the region over the continental shelf (depths less than 600 feet). Consequently, the elevations calculated by Adams were small and did not display the great variation along coastlines known to occur during historical tsunamis in the Hawaiian Islands.

Adams included the effects of propagation over continental shelves by multiplying the numerical model elevations by a factor (different for each island) that forced the best agreement with the historical

data. However, even with artifact, agreement with historical data was poor. For example, on the northeast coast of Oahu, the numerical model elevations multiplied by the factor resulted in predicted elevations ranging from 14 to 21.4 feet. Loomis (1976) presents 36 historical elevations for the 1946 Aleutian tsunami on the northeast coast of Oahu and only 7 even fall within this range of elevations. The historical elevations actually varied from 1 to 37 feet on this coast.

CHAPTER III

TSUNAMI INTERACTION WITH CONTINENTAL COASTLINES

Introduction

Experimental investigations of long wave interactions with continental coastlines have generally been one-dimensional and have involved idealized conditions. Flume tests by Savage (1958) and Saville (1956) measured runup of periodic waves on constant slope beaches and Hall and Watts (1953), Kaplan (1955), and Kishi and Saeki (1966) measured runup of solitary waves on constant slope beaches. All of these flume experiments used waves much steeper than typical tsunamis due to the difficulties involved in the generation of small amplitude long waves.

Many theoretical studies of one-dimensional propagation of weakly dispersive long waves have been performed in recent years. Tsunamis become weakly dispersive (amplitude and frequency dispersive) long waves at some point during their propagation, although (as was the case for the Hawaiian Islands) they may not be weakly dispersive for a time period sufficiently long for related effects to develop. The proper equations for the investigation of weakly dispersive long wave propagation over a steeply sloping bottom were first derived by Mei and LeMehaute (1966) and in a slightly different form by Peregrine (1967) who also gave the first numerical solution in the case of a solitary wave using an implicit finite difference

scheme. A more complete solution was later given by Madsen and Mei (1969) who transformed the equations to characteristic form before they were solved numerically. Svendsen (1974) studied weakly dispersive wave propagation over a gently sloping bottom. Hammack (1972) made comparisons of long wave generation by bottom displacements in the laboratory and numerical solutions of the Korteweg-DeVries equation using the numerical approach of Peregrine (1966).

Several studies of one-dimensional tsunami propagation over continental shelves of constant slope have been performed. Keller and Keller (1964) solved nonlinear long wave equations numerically for a constant slope bathymetry. Takahasi (1964) studied tsunami propagation over a simple bathymetry through analytic solutions of the linear long wave equation. Carrier (1966) assumed a tsunami was generated by a point source and studied nonlinear propagation over a constant slope bathymetry. Heitner and Housner (1970) used a finite element numerical method to solve nonlinear equations for propagation up constant slope beaches. More recently, Mader (1974) studied tsunami propagation over linear slopes using a finite difference solution of the complete Navier-Stokes equations (not vertically integrated).

Occasional two-dimensional studies have been performed for tsunami propagation in nearshore regions. Grace (1969) studied tsunamis affecting the reef runway of the Honolulu International Airport using a hydraulic model. However, the wavemakers used were only a small fraction of a tsunami wavelength from the region to be studied and waves reflected by land were reflected again almost

immediately by the wavemakers. This is a common problem in hydraulic model tests involving long waves. The wavemakers can be moved a few wavelengths from the region of interest by reducing the model scale; however, scale effects may then become very significant. Wave absorber screens may also be placed in front of the wavemakers; however, it is very difficult to absorb very long waves and such an approach is often not very helpful. Similar problems with re-reflected waves can occur in numerical studies. The calculations of Hwang and Divoky (1975) were in poor agreement with the tide gage recording of the 1964 tsunami at Hilo not only for the reasons presented in Chapter II, but also because their algorithm allowed waves to leave the numerical grid efficiently only for waves approaching the input boundary normally. Since Hilo Bay is triangularly shaped, the reflected waves approached the input boundary at various angles and were partially re-reflected toward Hilo.

Governing Equations

The governing equations for long wave propagation over the continental shelf of the west coast of the United States are Equations (2.3) and (2.4). Thus, the long wave assumption is made once again with vertical velocities and accelerations neglected relative to horizontal components. The continuity equation is given by the equation

$$\frac{\partial \eta}{\partial t} + \nabla \cdot \vec{q}(\eta + h) = 0 \qquad (3.1)$$

and the momentum equation is

$$\rho \frac{\partial \vec{q}}{\partial t} + \vec{q} \cdot \nabla \vec{q} = \rho F - \nabla p + \mu \nabla^2 \vec{q} \qquad (3.2)$$

If the only external force is gravity and the pressure is hydrostatic, then Equation (3.2) becomes

$$\rho \frac{\partial \vec{q}}{\partial t} + \vec{q} \cdot \nabla \vec{q} = \rho g \nabla \eta + \mu \nabla^2 \vec{q} \tag{3.3}$$

The west coast of the United States has a much broader continental shelf than that of the Hawaiian Islands; thus, the nonlinear advective and bottom stress effects may be more significant, and the nonlinear and viscous terms of Equation (3.3) must be retained.

The dynamic viscosity μ in the viscous term of Equation (3.3) is replaced by an eddy viscosity constant ε for the case of turbulent flow. Using this approach the viscous term can be expressed as

$$\varepsilon_1 \left(\frac{\partial^2 \vec{q}}{\partial x^2} + \frac{\partial^2 \vec{q}}{\partial y^2}\right) + \varepsilon_2 \frac{\partial^2 \vec{q}}{\partial z^2} \tag{3.4}$$

where the coefficients ε_1 and ε_2 represent coefficients of horizontal and vertical eddy viscosity, respectively. The term

$$\varepsilon_1 \left(\frac{\partial^2 q}{\partial x^2} + \frac{\partial^2 q}{\partial y^2}\right)$$

is usually small in comparison with the $\varepsilon_1 \frac{\partial^2 q}{\partial z^2}$ term (Dronkers, 1964) and will be neglected in this study. If $\varepsilon_1 \frac{\partial^2 q}{\partial z^2}$ is integrated with respect to z from the bottom to the surface and divided by the distance from bottom to surface $\eta + h$, we find

$$\frac{\varepsilon_2}{\eta + h} \left[\left(\frac{\partial u}{\partial z}\right)_{z=-h} - \left(\frac{\partial u}{\partial z}\right)_{z=\eta}\right] \tag{3.5}$$

The terms $\varepsilon_2 \left(\frac{\partial \mu}{\partial z}\right)_{z=-h}$ and $\varepsilon_2 \left(\frac{\partial u}{\partial z}\right)_{z=\eta}$ are components of the

tangential stresses at the sea bottom and surface, respectively. The shear stress at the sea surface is quite important for storm surge problems where wind velocities are very large but can be neglected relative to the bottom stress for tsunamis.

From experiments and theoretical considerations for one-dimensional flow in a river, it has been shown (Dronkers, 1964), that the bottom stress τ_b can be expressed as follows

$$\tau_b = \frac{-\rho g u|u|}{C^2} \tag{3.6}$$

where C is Chezy's coefficient and is given by the expression

$$C = \frac{1.486}{n_m} h^{1/6} \tag{3.7}$$

where n_m is Manning's n. Thus, Equation (3.3) may be written

$$\rho \frac{\partial \vec{q}}{\partial t} + \vec{q} \cdot \nabla \vec{q} = \rho g \nabla \eta - \frac{\rho g \vec{q} (u^2+v^2)^{1/2}}{C^2(\eta+h)} \tag{3.8}$$

Equation (3.8) contains the nonlinear advective term but neglects frequency dispersion since vertical accelerations have been neglected. This equation adequately describes wave propagation for Ursell numbers much greater than unity (Ursell, 1953). The Ursell number is proportional to the ratio of nonlinear effects to linear effects (i.e., frequency dispersion) and is equal to $\frac{\eta L^2}{h^3}$, where L is a typical wavelength. Since $L=(gh)^{1/2}T$ for long waves, where T is the wave period, an Ursell number may be chosen as $g\eta(\frac{T}{h})^2$. The numerical model described in the next section uses Equation (3.8) to propagate waves from depths of 500 meters to shore. These

waves have periods of the order of 1800 seconds and initial wave amplitudes of the order of a foot. Thus, the Ursell number, $gn(\frac{T}{H})^2$, is aproximately 30 and increases as the wave enters shallow water with h decreasing and η increasing.

Mader (1974) found that the one-dimensional form of Equation (3.8), without the viscous term, produced very similar results to a one-dimensional Navier-Stokes equation (viscosity neglected) for propagation of long wavelength tsunamis over linear continental slopes. The pressure term in Mader's solution was not hydrostatic; thus, frequency dispersion was permitted.

Finite Difference Model

To solve Equations (3.1) and (3.8) numerically, the differential equations are discretized and replaced by a system of finite difference equations using central differences on a space-staggered grid. The space-staggered scheme describes velocities, water levels, and depths at different grid points. This scheme, first used by Platzman (1958) for lake surge problems, has the advantage that in the equation for the variable operated upon in time, there is a centrally located spatial derivative for the linear term. Leendertse's (1967) implicit-explicit multi-operational method is employed in determining the solution for $\vec{q}$ and η as functions of time. The stability and convergence of this method is described in detail by Leendertse (1967). This method for solving finite-difference equations has been applied in studies analyzing the tidal hydraulics of harbors and inlets (Raney,

1976). Houston and Garcia (1975) used the method to calculate the decay of a tsunami as it enters and spreads throughout San Francisco Bay.

The nearshore finite-difference numerical model uses the time-history calculated by the generation and deep ocean propagation model described in Chapter II as input in the following manner. A tsunami is generated in the Aleutian-Alaskan area or the west coast of South America and propagated across the deep ocean to a 500-meter depth off the west coast of the United States. Waveforms calculated at this depth by the deep ocean numerical model are recorded all along the west coast. These waveforms are then used as input to the nearshore numerical model, which propagates the tsunamis from the 500-meter depths across the continental slope and shelf to shore.

Figure 13 shows outlines of the four numerical grids used to cover the west coast. The grids have square grid cells two miles on a side (southern California and some of San Francisco Bay were not covered by numerical grids because elevation predictions were made in previous studies (Houston and Garcia, 1974; and Houston and Garcia, 1975) using simple one-dimensional analytical solutions for propagation over the continental shelf). The offshore bathymetry was modeled from the 500-meter contour to shore. Beyond the 500-meter contour, the ocean was assumed to have a constant 500-meter depth. The input boundary of each grid was located approximately one and one-half wavelengths of a 30-minute wave from the shore. Therefore, at least three typical waves could arrive at the shore before waves reflected from the input boundary became a problem.

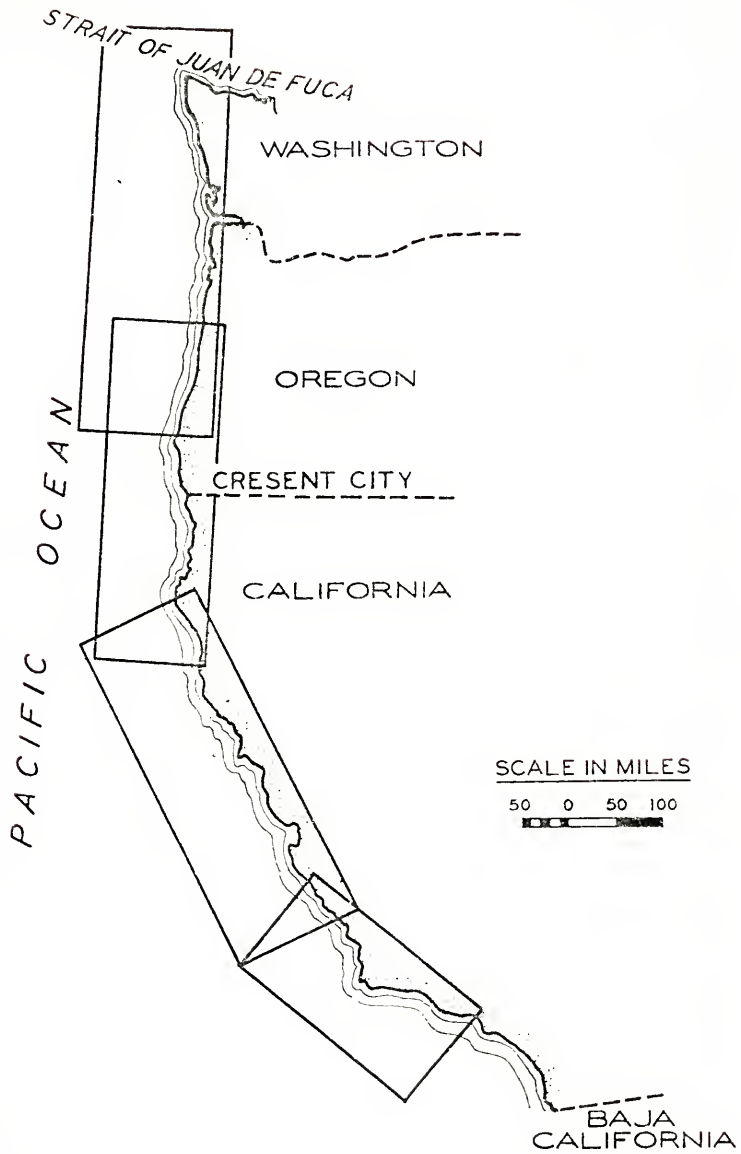

Figure 13. Finite Difference Grid Locations.

The input boundaries of the grids were oriented approximately parallel to the shoreline since refraction will bend the wavefronts to such an orientation before they reach the 500-meter contour (Wilson and Torum, 1968). Lateral boundaries of the grids were taken to be impermeable vertical walls.

Model Verification

The finite difference nearshore numerical model was also verified by numerical simulations of the 1964 Alaskan tsunami. The deep ocean propagation model discussed in Chapter II was used to generate the 1964 tsunami and propagate it across the deep ocean. Figure 14 shows surface elevation contours 3-1/2 hours after the 1964 Alaskan earthquake, as calculated by the deep-ocean propagation numerical model. This figure illustrates the concentration of energy on the northern California, Oregon, and Washington coasts due to the directional radiation of energy from the source region. The upper section of Figure 15 shows a time history of the 1964 Alaskan tsunami calculated by the deep-ocean model near Crescent City, California, in a water depth of 500 meters. This waveform was used as input to the finite difference nearshore model.

The lower section of Figure 15 shows a comparison between a tide gage recording of the 1964 tsunami at Crescent City and the nearshore model simulation of this tsunami. The numerical model calculations agree well with the tide gage recording; periods, phases, and amplitudes are accurately reproduced. The main disagreement occurs

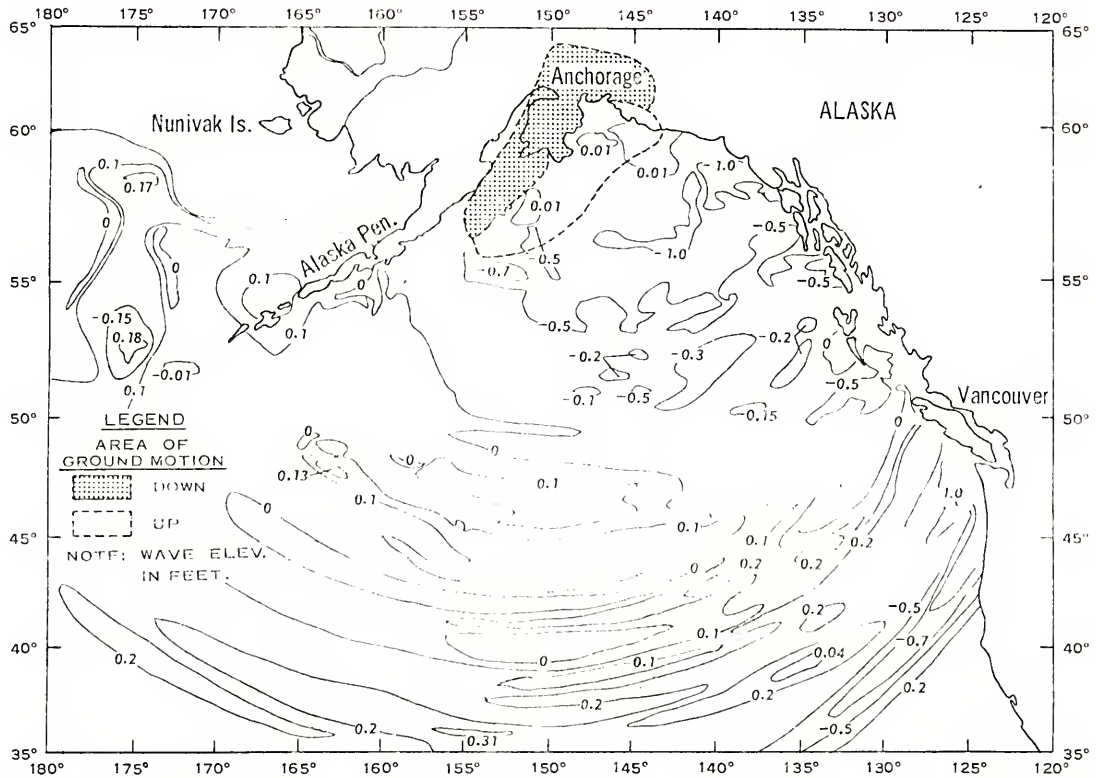

Figure 14. Wave Elevation Contours 3.5 Hours After 1964 Earthquake.

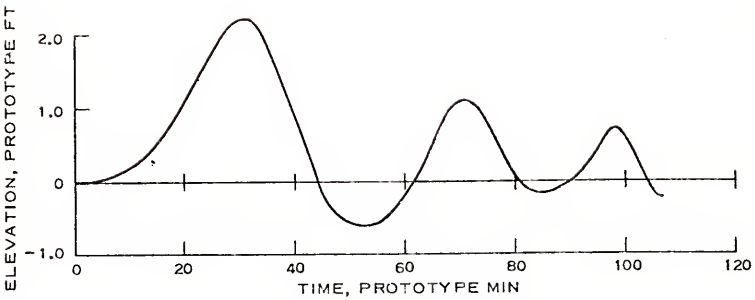

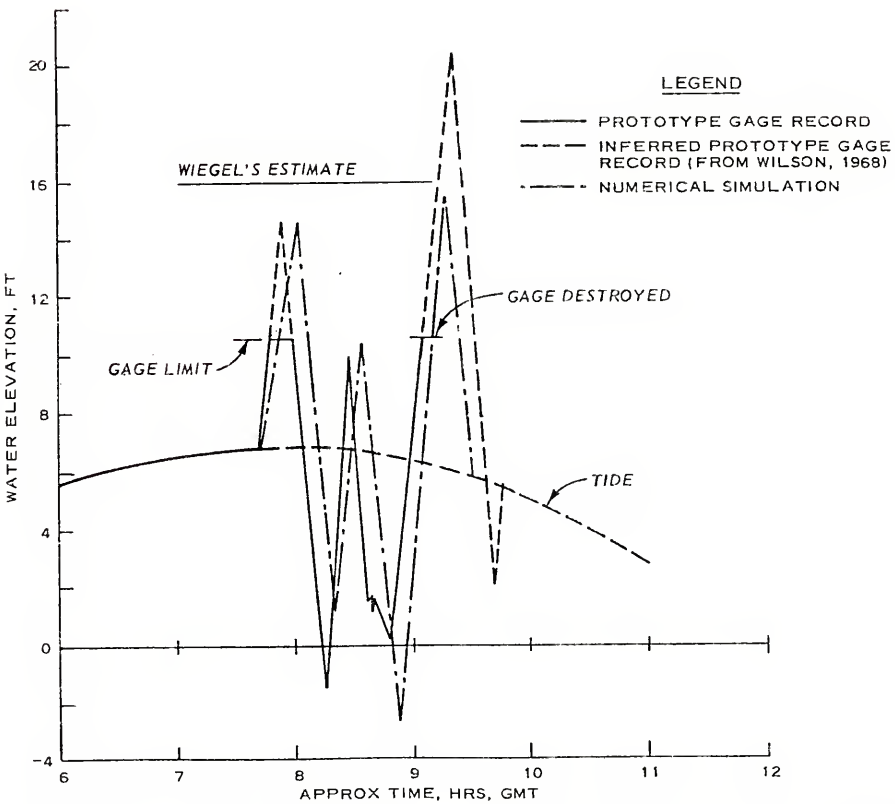

Figure 15. 1964 Tsunami from Alaska Recorded at Crescent City, California

for the amplitude of the third wave. With regard to this disagreement, it should be noted that there is also a lack of agreement on the amplitudes of the actual historical third and fourth wave crests. Figure 15 shows a reconstruction of the 1964 tsunami at Crescent City inferred by Wilson and Torum (1968) from the prototype gage record and later survey measurements by Magoon (1965). The elevation of the fourth wave (not shown) was estimated by Wilson and Torum to have been a little less than 14 feet above mean lower low water (MLLW) (the zero elevation shown in Figure 15 is MLLW datum); however, Wiegel (1965) estimated that the elevation of the third wave was approximately 16 feet above MLLW and that the fourth wave attained the highest elevation of 18 or 19 feet above MLLW at the tide gage location. The numerical model predicted a fourth wave elevation approximately the same as that estimated by Wilson and Torum (14 feet above MLLW). However, reflections from the input boundary were probably growing in importance in the numerical model calculations during the arrival of the fourth wave.

There may be several reasons why the maximum wave elevation predicted by the numerical model does not agree with the historical record as well as the elevations of the initial waves. First, the later waves in the deepwater waveform are probably waves which have been reflected from land areas in the source region. The fairly large grid cell spacing used in the deep ocean propagation model to represent the land-water boundary in this region probably distorts the reflected waveform. Total reflection of waves in this region also is not completely realistic. Furthermore, the nearshore grid may

not have fine enough cells to completely model the resonance phenomenon leading to the large third or fourth wave.

Since 1964, there has been considerable speculation concerning the reasons that the effects of the 1964 tsunami were so great at Crescent City. The finite difference numerical models show that both the directional radiation of energy from the source region (see Figure 14) and a local resonance caused the relatively large elevations at Crescent City. Actually, large elevations at Crescent City were not unique since directional radiation of energy from the source also caused large elevations along the Oregon and northern California coasts. Runup 10 to 15 feet above the high tide level occurred all along the Oregon coast south of the Columbia River (runup at Crescent City was approximately 15 feet above the high tide level). However, the Oregon coast is very sparsely populated and there were few damage reports. The severity of structural damage at Crescent City, which has a large logging industry, also was apparently due to the impact of logs carried by the tsunami (Wilson and Torum, 1968). The nearshore numerical model indicates that the resonant effects at Crescent City were fairly local, extending over 2 to 4 miles of coastline. This behavior contradicts Wilson and Torum's (1968) speculation that a bowl-shaped section of the continental shelf with a diameter of approximately 50 miles experienced a resonant oscillation. Historical data support the numerical model calculations. At the mouth of the Klamath River, approximately 15 miles south of Crescent City, elevations observed during the 1964 tsunami were only 2 to 3 feet above normal high

tide. Wilson and Torum's hypothesis of a shelf oscillation would predict elevations at the mouth of the Klamath River greater than those that occurred at Crescent City.

Figure 16 shows a comparison between a tide gage recording of the 1964 tsunami at Avila Beach, California, and the nearshore numerical model calculations. The elevations recorded by the Avila Beach tide gage were larger than those recorded at any tide gage on the west coast except the Crescent City gage. The historical and calculated waveforms shown in Figure 16 are in good general agreement. The tide gage record obviously has higher frequency components which are not predicted by the numerical model; these components may be local oscillations of water areas which were too small to be accurately represented by the numerical grid. Important features such as the wave amplitudes are in good agreement.

The waveforms recorded for the 1964 tsunami by the Crescent City and Avila Beach tide gages have elevations larger than those recorded by any other gage on the west coast. Other tide gage recordings of this tsunami on the west coast (except at Astoria, Oregon) were in areas not covered by the grids shown in Figure 13. A comparison with the tide gage at Astoria, Oregon, was not made because Astoria is approximately 12 miles away from the coast in the estuary of the Columbia River, and amplitudes of the 1964 tsunami were small at Astoria.

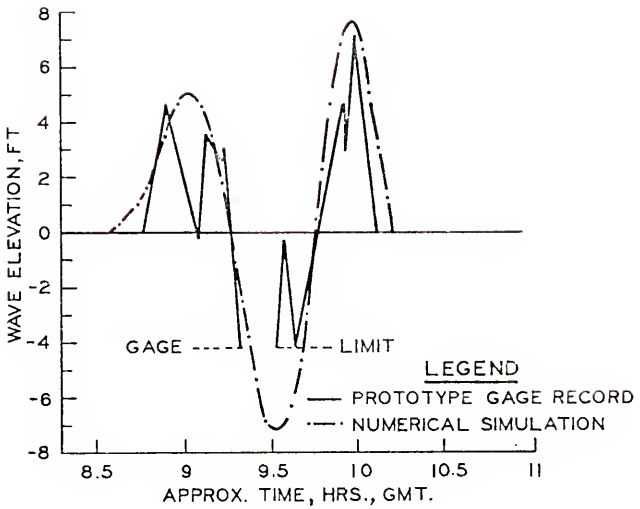

Figure 16. 1964 Tsunami from Alaska Recorded at Availa Beach, California.

CHAPTER IV

ELEVATION PREDICTIONS

Hawaiian Island Predictions

Introduction

The Hawaiian Islands, a chain of eight islands as shown in Figure 17, have a history of destructive tsunamis generated both in distant areas and locally. The earliest recording of a severe tsunami in the Hawaiian Islands was in 1837 when a tsunami from Chile reached an elevation of 20 feet at Hilo, Hawaii, and killed 46 people in the Kau District of the big island of Hawaii. Prior to 1837, a number of severe tsunamis undoubtedly reached the islands but, unfortunately no detailed records were kept. Since 1837, there have been 16 tsunamis that have caused significant damage.

Most of the destructive tsunamis in the Hawaiian Islands have been generated along the coast of South America, the Aleutian Islands, and the Kamchatkan Peninsula of the Soviet Union. Approximately one-fourth of all the tsunamis recorded in the Hawaiian Islands have originated along the coast of South America, while more than one-half have originated in the Kuril-Kamchatka-Aleutian region of the north and northwestern Pacific. Tsunamis generated by local seismic events have caused large runup in the islands, especially on the southeast coast of the big island of Hawaii. The 1868 tsunami produced the largest waves of record in the Hawaiian Islands with

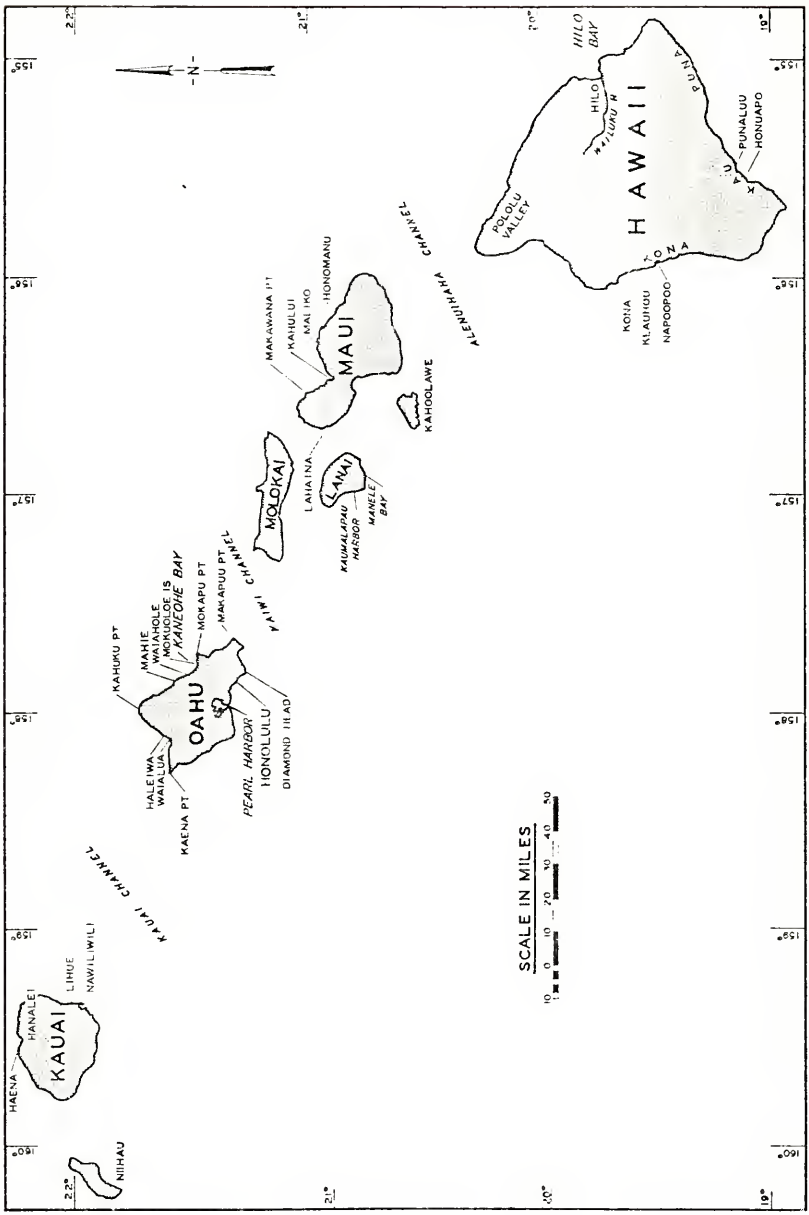

Figure 17. Hawaiian Islands.

60-foot waves reported on the South Puna coast of the island of Hawaii. The most recent major tsunami in Hawaiian history occurred on November 29, 1975, when waves generated by an earthquake with an epicenter on the South Puna Coast may have reached elevations as great as 45 feet along the southeast coast. The most destructive tsunami to ever hit the islands in terms of both loss of life and property destruction was the Great Aleutian tsunami of 1946, which killed 173 people and produced waves over 55 feet in elevation. Hilo incurred $26 million in property damage attributable to this tsunami. The 1960 Chilean tsunami is the most recent distantly generated tsunami that produced major effects in the Hawaiian Islands. Sixty-one lives, all at Hilo, were claimed by the tsunami. Damage throughout the state was estimated to be $23.5 million. Inspection of the damage at Hilo revealed much evidence of the tremendous forces developed by the waves. Twenty-ton boulders had been moved hundreds of feet, asphaltic concrete pavements were peeled from their subbase, and hundreds of automobiles were moved and crushed.

The following sections discuss the methods used to obtain sufficient data to predict runup elevations for the entire coastline of the Hawaiian Islands. The finite element numerical model discussed in Chapter II is used to interpolate between local historical data for the years of accurate survey measurements from 1946 through 1977. Such a method of interpolation is needed so that elevations can be predicted for the entire coastline even for locations having no actual historical data. A method is discussed herein which allows reconstruction of historical data for the period of time from 1837 to

1946 when elevations for the period from 1946 through 1977 are known. Such an approach is necessary in order to have sufficient data for accurate elevation predictions since it is shown herein that reasonable predictions cannot be made solely based upon known historical data for the short time span from 1946 through 1977.

Interpolation of Recent Historical Data

Historical data of tsunami activity in the Hawaiian Islands are, of course, often limited to certain locations. Information on tsunami activity in the islands prior to the 1946 tsunami is concentrated in Hilo (Hawaii) and to a lesser extent in Honolulu (Oahu) and Kahului and Lahaina (Maui). Even data for tsunamis occurring during the period of accurate survey measurements from 1946 through the present are absent or fragmentary (i.e., data exist only for certain of the events) for most of the coastline of the islands. Therefore, it is necessary to rely on more than just available historical data to determine tsunami occurrence frequencies.

The numerical model is used to fill in historical data gaps for tsunamis from 1946 through 1977 by providing relative responses of the Hawaiian Islands to tsunamis. For example, although the deepwater waveform of a tsunami such as that of 1946 is not known, the direction of approach of this tsunami and its range of wave periods are known. The average response of the islands to a tsunami similar to the 1946 tsunami is determined by inputting sinusoidal waves of unit amplitude from the direction of the 1946 tsunami into the numerical model over a band of wave periods. If historical data exist at one location, wave elevations at a nearby location for which historical data do not exist are determined by multiplying the historical data at the

first location by the ratio of the response calculated by the numerical model at the second location and the response calculated at the first. The numerical model takes into account the major processes that would cause different relative wave elevations at the two locations. That is, the model calculates shoaling, refraction, diffraction, reflection, resonance, shielding of the backside of an island by the front side, and interactions between islands. The historical data account for the unknown absolute heights of the deepwater tsunamis. The "correction factors" provided by the historical data are local instead of global (single factor for all islands) because there are certain local factors that cannot be determined by the numerical model. For example, coral reefs extend over parts of some of the islands and are known to protect against tsunami attack (e.g., the extensive reefs in Kaneohe Bay, Oahu, which are powerful tsunami dissipators). The effects of the reefs on tsunamis are implicitly contained in the historical data itself. The historical data from 1946 through the present were taken from the most recent and complete compilation of these data (Loomis, 1976).

As an example of the use of the numerical model to fill in historical data gaps for tsunamis from 1946 through the present, consider the 1946 tsunami recorded on the island of Lanai only at Kaumalapua Harbor and Manele Bay. Wave elevations can be calculated for the 1946 tsunami at other locations on the coastline of Lanai by multiplying these historical values by the ratios of the responses calculated by the numerical model at locations of interest and the responses calculated at Kaumalapua Harbor and Manele Bay. In this

way, elevations for the 1946 tsunami can be determined for all of Lanai.

Time Period Analysis

It is necessary to use historical data of tsunami occurrence covering the greatest possible time span to properly determine frequency of occurrence of tsunami elevations for the Hawaiian Islands. Tsunami activity has not been uniform in these islands during recorded history. For example, the two largest and four of the ten largest tsunamis striking Hilo from 1837 through 1977 occurred during the 15-year period from 1946 through 1960. Two of the tsunamis from 1946 through 1960 originated in the Aleutian Islands, one in Kamchatka and one in Chile. However, six of the ten largest tsunamis occurred during the 109-year period from 1837 to 1945 with three originating in Chile, two in Kamchatka and one in Hawaii. Therefore, both the frequency of occurrence and place of origin of tsunamis have been remarkably variable. Any study (e.g., Towill Corporation, 1975) basing frequency calculations on a short time span that includes the period from 1946 through 1960 will predict a significantly more frequent occurrence of large tsunamis than is warranted by historical data from 1837 through 1977.

The errors introduced in frequency of occurrence calculations by consideration only of a short time period that includes the unrepresentative years from 1946 through 1960 will be greater than the errors resulting from possible observational inaccuracies of the 19th Century. This is easily demonstrated for Hilo, Hawaii, which is the location in the Hawaiian Islands having the most complete

data of tsunami activity. Using the data compiled by Cox (1964) for the ten largest tsunamis in Hilo from 1837 through 1977 (his data were actually through 1964, but no large tsunamis have occurred in Hilo since 1964), a least-squares fit of the data was made employing the logarithmic frequency distribution discussed later in this chapter. The 100-year tsunami elevation for Hilo calculated using this method was 27.3 feet. If the elevations recorded during the nineteenth centry (five of the ten largest tsunamis), are increased by 50 percent (which is much larger than possible observational error), the 100-year elevation is found to be 30.4 feet. Similar calculations just based upon data taken during the period of accurate survey measurements in Hilo from 1946 through 1977 yields a 100-year elevation of 44.2 feet. Since the largest elevation in Cox's data for the 141-year period from 1837 through 1977 was just 28 feet, the 100-year elevation of 44.2 feet is obviously too large. Similar overestimates will occur at any location in the Hawaiian Islands if an analysis is based upon a short period of time that includes the years 1946 through 1964 since the exceptionally frequent occurrence of major tsunamis in Hilo from 1946 through 1964 is a property of the unusual activity of tsunami generation areas and not of special properties of Hilo.

The unusual tsunamigenic activity in generation regions in recent years is reflected in the most up-to-date catalog of tsunami occurrence in the circumpacific area complied by Soloviev and Go (1969). This catalog shows, for example, that the three greatest intensity tsunamis generated in the Aleutian-Alaskan region since

1788 occurred in 1946, 1957, and 1964. The catalog also lists the 1960 Chilean tsunami as the greatest intensity tsunami generated in South America in recorded history (416-year period from 1562 through 1977). Reporting of tsunamis on the west coast of South America is quite good with 105 tsunamis reported during the 416-year period. Kanamori (1977) also notes the unusual seismic activity that occurred during a relatively short time span in recent years. He shows that the four earthquakes having the greatest seismic moments (true measure of magnitude for great earthquakes) in this century occurred during a thirteen year period from 1952 through 1964 (1960 Chilean, 1964 Alaskan, 1957 Aleutian, and 1952 Kamchatkan earthquakes).

Evidence that tsunamis were unusually active in the Hawaiian Islands from 1946 through 1964 is also apparent from historical data at Kahului and Lahaina, Maui. Kahului, Lahaina, Hilo, and Honolulu are the only locations in the islands with historical data extending to 1837. Four of the five largest tsunami elevations recorded at Kahului occurred during the years from 1946 through 1964. Three of the four largest tsunami elevations recorded at Lahaina occurred during the same period. The historical data for Honolulu is not very useful because the commonly reported elevations for the 1837 and 1841 tsunamis were, in fact, drops in water level (Pararas-Carayannis, 1977) and there are no reports for the 1868 and 1877 tsunamis from Chile.

Reconstruction of Historical Data

In order to have data covering a sufficiently long time span to make reasonable predictions of tsunami elevations for the Hawaiian Islands, it is necessary to reconstruct historical data for the

years prior to 1946. To do this, it is assumed in this study that tsunamis generated in a single source region (Kamchatka or Chile but not the Aleutian-Alaskan region) approach the islands from approximately the same direction and have energy lying within the same band of wave periods. The difference in wave elevations at the shoreline in the Hawaiian Islands produced by tsunamis generated at different times in the same region is attributed mainly to differences in deepwater wave amplitudes. For example, the 1841 tsunami from Kamchatka produced a wave elevation in Hilo that was approximately 25 percent greater than that of the 1952 tsunami from Kamchatka. It is assumed that these two tsunamis had the same relative magnitudes throughout the islands. Since the finite element model allows a determination of elevations for the 1952 tsunami along the entire coastline of the islands, the elevations of the 1841 tsunami and all other Kamchatkan tsunamis occurring during the period of record in Hilo from 1837 to 1946 can be reconstructed for the entire coastline. Similarly, Chilean tsunami elevations can be reconstructed knowing elevations for the 1960 Chilean tsunami. No major tsunamis were generated in the Aleutian-Alaskan region from 1837 through 1946; hence, no reconstruction is necessary for tsunamis from this region. Fortunately, tsunamis from this region since 1946 were representative of the entire region since these tsunamis were generated in the western Aleutians (1957), central Aleutians (1946) and eastern Alaskan area (1964).

The assumption that tsunamis generated in a single source region (Kamchatka or Chile) approach the Hawaiian Islands from

nearly the same direction is justified in the case of Kamchatka by the small spatial extent of the known generation area. However, the tsunamigenic area of Chile is considerably larger than that of Kamchatka. Still, the direction of approach of different tsunamis from Chile is nearly the same because the tsunamigenic region in Chile subtends a relatively small angle with respect to the islands as a result of the great distance between Chile and the Hawaiian Islands and the axis of the Chile Trench maintains a constant orientation relative to the islands (thus directional radiation effects are not important).

The assumption that tsunamis generated in a single source region have energy lying within the same band of wave periods is supported by the elevation patterns produced along coastlines in the Hawaiian Islands by different historical tsunamis. These patterns are such that it has been concluded that "tsunamis of diverse geographic origin are strikingly different, whereas those from nearly the same origin are remarkably similar" (Eaton, et al., 1961). A recent study by Wybro (1977) shows that even the distributions of normalized elevations (i.e. the elevation patterns) produced in the Hawaiian Islands by different Aleutian-Alaskan tsunamis are nearly the same yet quite different from the distributions for tsunamis of other origins. This agreement occurs dispite the fact that the relatively close proximity to Hawaii of the Aleutian-Alaskan Trench and the varying orientation of the trench axis relative to Hawaii introduces important directional effects for tsunamis generated in the Aleutian-Alaskan area. Apparently, these directional effects influence the

magnitude of the elevations in Hawaii but do not greatly alter elevation patterns. Therefore, historical observations support the approach used in this study which estimates the elevations produced by tsunamis from Chile or Kamchatka prior to 1946 based upon data for tsunamis from these tsunamigenic regions recorded during the years of accurate survey measurements from 1946 to 1977.

In this study elevations are calculated along the coastline of the Hawaiian Islands for the ten tsunamis which produced the greatest elevations in Hilo, Hawaii, from 1837 through 1977. The finite element numerical model fills in all data gaps for those tsunamis of the ten that occurred from 1946 through 1977 and then the Hilo data (Cox, 1964) is used to determine relative magnitudes to reconstruct the elevations for those tsunamis that occurred prior to 1946. For much of the coast of the Hawaiian Islands, the ten largest tsunamis since 1837 would be the same as the ten largest tsunamis in Hilo for the same period. That is, the ten largest would be the tsunamis of 1960, 1946, 1923, 1837, 1877, 1841, 1957, 1952, and the two in 1868. Of course, the order of the ten largest would vary from location to location. For example, the largest tsunami on the South Puna coast of the big island of Hawaii was the locally generated tsunami of 1868.

There are a few locations where historical data show that one of the ten largest tsunamis was not among the ten largest in Hilo from 1837 through 1977. For example, the 1896 tsunami generated near Japan produced small elevations in the Hawaiian Islands except at Keauhou on the Kona coast of the big island of Hawaii. The

observation at Keauhou was, therefore, included in the frequency of occurrence analysis for that location. Similarly, all other historical observations of significant tsunami elevations at isolated locations were included in the frequency of occurrence analyses for those locations. Historical data for tsunamis prior to 1946 were taken from Pararas-Carayannis (1977). Data for the local tsunami of November 29, 1975, were taken from the compilation by Loomis (1976). Since the local tsunami of 1868 had an earthquake epicenter very near that of the 1975 tsunami and the two apparently produced very similar elevation patterns (Tilling et al., 1976), historical elevations for the two tsunamis recorded at the same location were used to determine a relative magnitude of the tsunamis. The many observations for the 1975 tsunami were then used to reconstruct elevations for the 1868 tsunami.

Frequency of Occurrence Distribution

After the ten largest tsunamis from 1837 through 1977 were determined at locations all along the coasts of the Hawaiian Islands using the methods discussed in the previous sections, elevation versus frequency of occurrence curves were determined at each location by least-squares fitting of the data by the following expression:

$$h = -B - A \log_{10} f \qquad (4.1)$$

where

h = elevation of maximum wave at the shoreline,

f = frequency per year of occurrence.

Equation (4.1) was used as the frequency of occurrence distribution

since it has been found to agree with historical data at several locations. Cox (1964) found that the logarithm of tsunami frequency of occurrence was linearly related to tsunami elevations for the ten largest tsunamis occurring from 1837 through 1964 at Hilo, Hawaii. Soloviev (1969) has shown a similar relationship between tsunami frequency of generation and intensity for moderate to large tsunamis. Also, earthquake frequency of occurrence and magnitude have been similarly related by Gutenberg and Richter (1965); Wiegel (1965) found the same relationship for historical tsunamis at San Francisco and Crescent City, California and Adams (1970) for tsunamis at Kahuku Point, Oahu. A recent study by Rascon and Villarreal (1975) revealed the same relationship for historical tsunamis on the west coast of America, excluding Mexico.

It is possible that other distributions may agree with the historical data equally well as the logarithmic distribution. For example, the Gumbel distribution has been used in the past to study annual streamflow extremes (Gumbel, 1955). Borgman and Resio (1977) illustrate the use of this distribution to determine frequency curves for non-annual events in wave climatology. To investigate the sensitivity of calculations of 100-year elevations on the assumed frequency distribution, the approach of Borgman and Resio was applied to the Hilo data of Cox. The Gumbel distribution yields a 100-year elevation of 28.8 feet for data from 1837 through 1977 and an elevation of 42.5 feet for data from 1946 through 1977. This compares with the elevations of 27.3 feet and 44.2 feet calculated for the same time periods using the logarithmic distribution (Equation (4.1)). Clearly, the arguments used earlier concerning the period of time that must be considered for

a valid analysis are not dependent upon the assumed frequency distribution. Since ample precedent exists for using the logarithmic distribution for analyzing tsunami frequency of occurrence, this distribution is used in this study.

Results

The methods described in the previous sections allow frequency of occurrence curves to be constructed for points all along the coastline of the Hawaiian Islands. The coefficients A and B of Equation (4.1) contain all necessary information to determine frequency of occurrence of tsunami elevations at a location. Plots of the coefficients A and B versus location along the coasts were constructed for all of the islands. Smooth curves were drawn through these coefficients to allow elevation predictions at any location. Figures 18 and 19 show typical plots of A and B for the southeastern coast of the big island of Hawaii (Figure 20). For example, at Hoopuloa (location 11 in Figure 20) A = 6 and B = 4; hence, the 100-year elevation (F = .01) is only 8 feet. The 100-year elevations for most locations in the Hawaiian Islands are considerably larger.

For such situations involving human life, one is less interested in the mean exceedance frequency f (the average frequency per year of tsunamis of equal or greater elevations) than in the chance of a given elevation being exceeded in a certain period of time. To calculate risk, one first notes that tsunamis are usually caused by earthquakes, and earthquakes are often idealized as a generalized Poisson process (Newmark and Rosenblueth, 1971 and Der Kiureghian and Ang, 1977). It was assumed by Wiegel (1965) and Rascon and

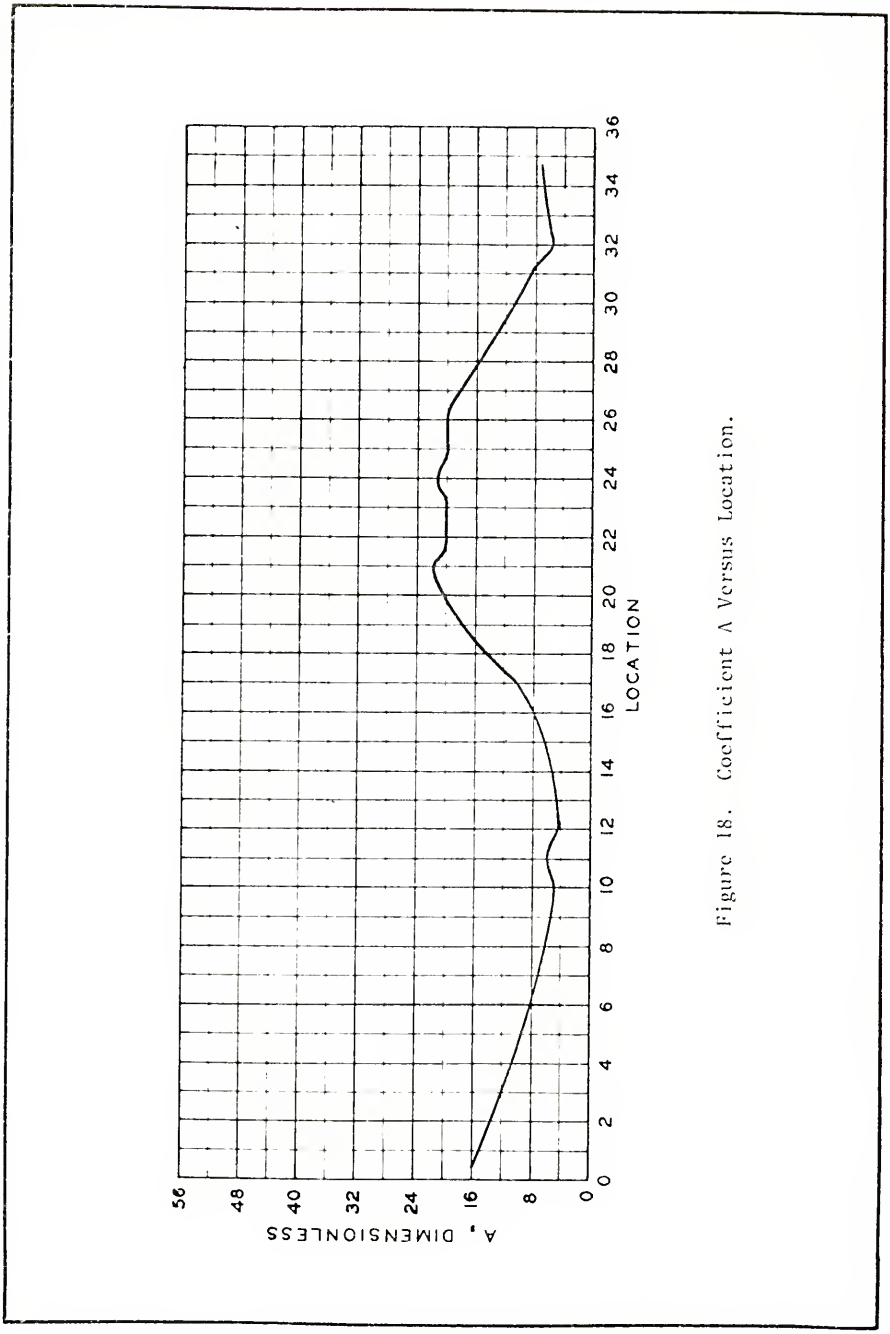

Figure 18. Coefficient A Versus Location.

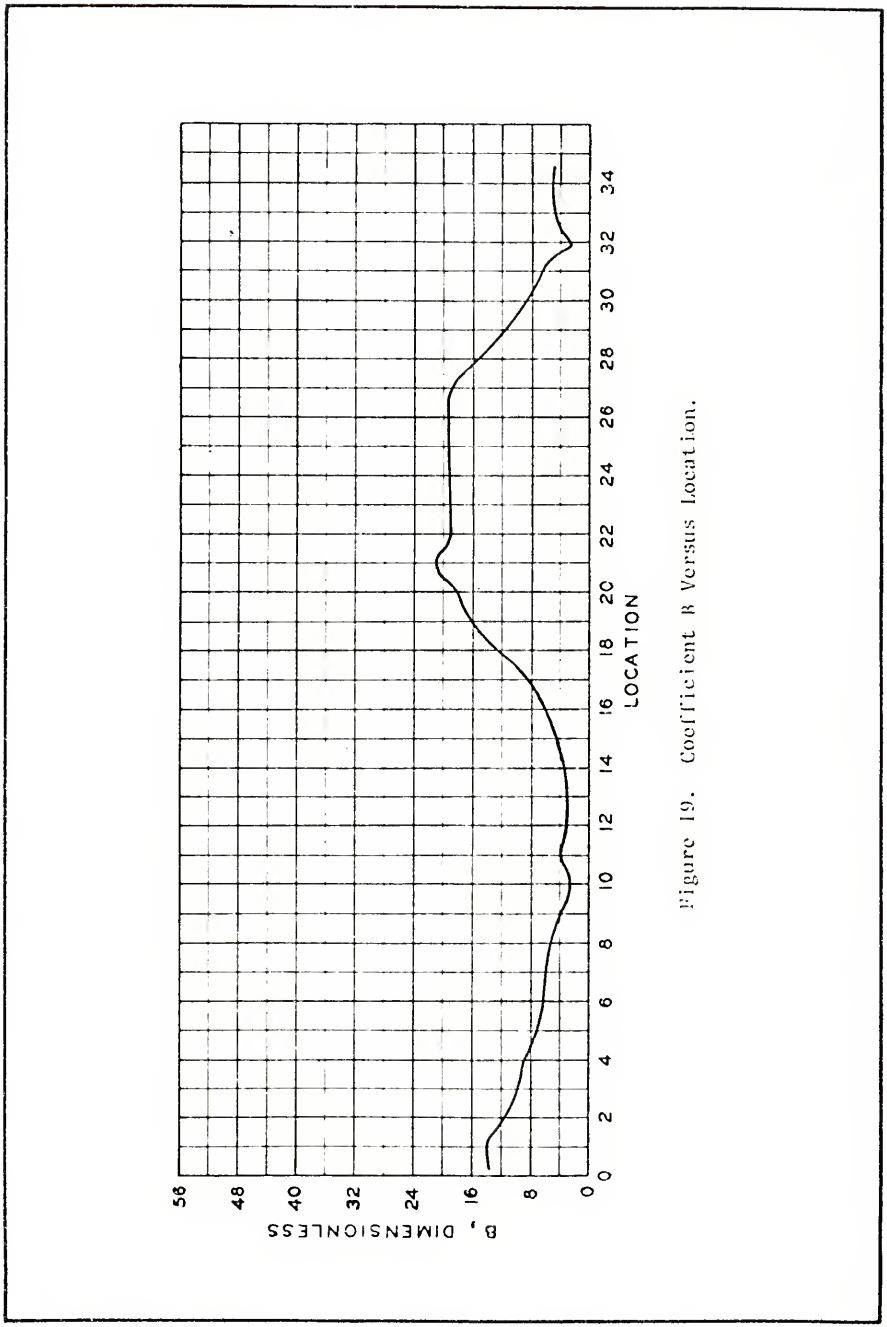

Figure 19. Coefficient B Versus Location.

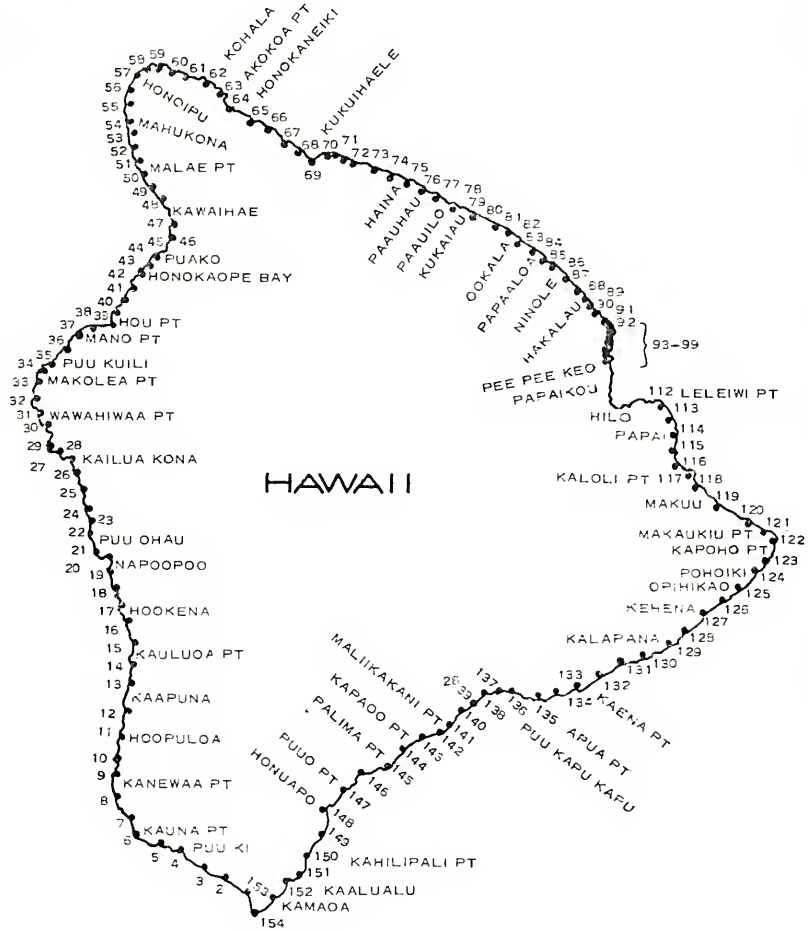

Figure 20. Location Map for Hawaii.

Villarreal (1975) that tsunamis also follow such a stochastic process. The probability that a tsunami with an average frequency of occurrence of f is exceeded in D years, assuming that tsunamis follow a Poisson process, is given by the following equation:

$$P = 1 - e^{-fD} \tag{4.2}$$

Thus, if an acceptable risk is one chance in one thousand that an elevation be exceeded during a 100-year period, $P = .001$ and $D = 100$ years. Substituting these values in Equation (4.2) yields the elevation h which has one chance in one thousand of being exceeded during the next 100 years.

West Coast of the United States Predictions

Introduction

Unlike the Hawaiian Islands, the west coast of the continental United States lacks sufficient data to allow tsunami elevation predictions based upon local historical records of tsunami activity. Virtually all of the west coast is completely without data of tsunami occurrence, even for the prominent 1964 tsunami. Only a handful of locations have historical data for tsunamis other than the 1964 tsunami. However, the Federal Insurance Administration requires information on tsunami elevations for the entire west coast of the continental United States; even for the many locations that have no known historical data of tsunami activity and for coastal areas that are currently not developed (since these areas may be developed in the future). The lack of historical data of tsunami activity on the west coast

necessitates the use of numerical models to predict runup elevations. The Aleutian-Alaskan area and the west coast of South America were found by Houston and Garcia (1974) to be the tsunamigenic regions of concern to the west coast of the United States. Both regions have sufficient data on the generation of major tsunamis to allow a statistical investigation of tsunami generation. The generation and deep-ocean propagation model described in Chapter III can then be used to generate representative tsunamis and propagate them across the deep ocean. The nearshore numerical model also described in Chapter III, can then be used to propagate tsunamis from the deep ocean over the continental slope and shelf to shore.

In this study, only tsunamis of distant origin are considered in the analysis. Hammack (1972) has shown that near the generation region of an impulsively generated tsunami, the waveform is dependent upon details of the time-dependent movement of the ground during the earthquake. Little is known about the actual time-dependent ground motion during earthquakes generating tsunamis and this motion cannot be predicted in advance. Also, there is not enough historical data concerning locally generated tsunamis on the west coast to allow predictions of tsunami occurrence. Thus, reasonable predictions on the west coast of the properties of locally generated tsunamis or their likelihood of occurrence are not possible at this time.

The probability is not considered very great that a destructive, locally generated tsunami will occur on the west coast of the continental United States. Tsunamis are generally produced by earthquakes having fault movements that exhibit a pronounced "dip-slip," or

vertical component of motion. "Strike-slip," or horizontal displacement, fault movements are inefficient generators of tsunamis. Faults on the west coast of the United States characteristically exhibit "strike-slip" motion since the Pacific block of the earth's crust is moving horizontally relative to the North American block. The west coast of the United States does not share the characteristics (ocean trenches and island arcs) of known-generating areas and, in fact, has not historically been one. Relatively small locally generated tsunamis have been known to occur on the west coast, but there are no reliable reports of major locally generated tsunamis. Heights of 6 feet in the immediate vicinity of the 1927 Point Arguello earthquake are the largest authenticated heights produced by local tsunamis on the west coast). There could be a few locations on the west coast for which locally generated tsunamis pose a greater hazard than do distantly generated tsunamis because the elevations produced by distantly generated tsunamis are small. However, predictions of elevations produced by locally generated tsunamis are beyond the scope of this study.

Tsunami Occurrence Probabilities

Historical data of tsunami generation must be the basis for an analysis that considers the probability of tsunami generation in the two tsunamigenic regions of the Pacific Ocean of concern to the west coast of the continental United States--the Aleutian and Peru-Chile Trench regions. A satisfactory correlation between earthquake magnitude and tsunami intensity has never been demonstrated. Not all large earthquakes occurring in the ocean even generate noticeable

tsunamis. Furthermore, earthquake parameters of importance to tsunami generation, such as focal depth, rise time, and vertical ground displacement, have only been measured for earthquakes occurring in recent years. Therefore, data of earthquake occurrence cannot be used to determine occurrence probabilities of tsunamis. Instead, historical data of tsunami occurrence in generation regions must be used to determine these probabilities.

In South America, a wealth of information exists concerning tsunami generation. Reliable data (grouped in intensity increments of one-half) exist for tsunamis with intensity greater than or equal to 0 for a 171-year period and greater than or equal to 2-1/2 for a 416-year period (Soloviev and Go, 1969). The intensity scale used is a modification (by Soloviev and Go) of the standard Imamura-Iida tsunami intensity. Intensity is defined as

$$I = \log_2(\sqrt{2}\, H_{avg}) \tag{4.3}$$

This definition in terms of an average runup (in meters) over a coast instead of a maximum runup elevation at a single location (used for the standard Imamura-Iida scale) tends to eliminate any spurious intensity magnitudes caused by often observed anomalous responses (due, for example, to local resonances) of single isolated locations.

Using the most recent and complete catalog of tsunami occurrence in the Pacific Ocean (Soloviev and Go, 1969) a relationship between tsunami intensity and frequency of occurrence was determined for the tsunamigenic trench running the length of the Peru-Chile coast. Tsunamis with intensity greater than or equal to 0 were considered.

It was assumed that the logarithm of the tsunami frequency of occurrence was linearly related to the tsunami intensity. Earlier in this chapter, it was shown that such a relationship holds between both earthquake magnitude and frequency of occurrence and tsunami intensity and frequency of occurrence.

Letting $n(I)$ equal the probability of a tsunami with an intensity I being generated during any given year and using statistics for the entire trench along the Peru-Chile coast, a least-squares analysis results in the following expression:

$$n(I) = 0.74e^{-0.63I} \tag{4.4}$$

In using statistics for the entire trench area along the Peru-Chile coast, it is assumed that the probability of tsunami occurrence is uniform along the trench. This is a standard assumption for earthquake frequency analysis (Gutenberg and Richter, 1965). The tectonic justification of this assumption lies in the fact that a single Sialic block or plate of the earth's crust or lithosphere is dipping into the Peru-Chile Trench (Wilson, 1959). It can reasonably be expected that the movement of this single plate is similar along its entire length.

In the Aleutian Trench region, only large tsunamis occurring in relatively recent years (since 1788) have been recorded due to the isolation of the area. Assuming an exponential coefficient of -0.71 for this trench area (determined by Soloviev, 1969) as a mean value for regions of the Pacific with the most data on tsunamis) and using only the reliable data for large tsunamis (intensity greater than or equal to 3.5) from Soloviev and Go (1969), the following relationship

is determined by a least-squares analysis:

$$n(I) = 0.113e^{-0.71I}$$

Again, the probability of tsunami occurrence is assumed to be uniform along the trench.

Use of Deterministic Numerical Models

To relate the probability distributions of tsunami intensities to source characteristics, it is assumed that the ratio of the source uplift heights producing two tsunamis of different intensity (as defined in the previous section) is equal to the ratio of the average runup heights produced on the coasts near these tsunami sources. This ratio is equal to $2^{|I_1-I_2|}$ for two tsunamis with intensities I_1 and I_2

If H_a is the wave height in the direction parallel to the major axis of length a of a tsunami source with an elliptical shape (large tsunamis have historically had elliptically-shaped uplifts) and H_b is the wave height in the direction parallel to the minor axis of length b, then experimental research of tsunami generation has shown that H_b/H_a is approximately equal to a/b (Hatori, 1963). For a large tsunami, H_b can be larger than H_a by a factor of as much as 5 or 6. Thus, the orientation of the tsunami source relative to the area where runup is to be determined is very important, i.e., the runup at a distant site due to the generation of a tsunami at one location along a trench cannot be considered as being representative of all possible placements of the tsunami source in the entire trench region. Hence, the Aleutian and Peru-Chile Trenches had to be segmented and runup along the west coast of the United

States determined for tsunami sources located at the center of each of the segments.

The spatial size of a tsunami source was standardized since there is not an apparent correlation between tsunami intensity and spatial size of a tsunami source. For example, the 1946 Aleutian tsunami had an uplift region of very small spatial extent, whereas the 1957 Aleutian tsunami had an uplift region that covered perhaps the greatest spatial extent of any known earthquake (Kelleher, 1972). Yet the 1946 tsunami had the greater intensity, producing, in general, greater runup elevations in the near and distant regions. The standard source used is discussed in detail by Houston and Garcia (1974). It is elliptical in plan view with a major axis length of 600 miles and a minor axis length of 130 miles. The vertical displacement increases linearly from a zero elevation on the ellipse perimeter to a maximum displacement of 30 feet. The vertical displacement has a parabolic crest (concave downward) parallel to the direction of the major axis. The standard source represents a large tsunami with intensity 4 on the modified Imamura-Iida scale. Certainly, tsunamis of low intensity may have smaller spatial extents; however, large tsunamis pose the greatest threat to a distant area such as the west coast of the United States. These large tsunamis can be expected to have similar spatial extents, with any spatial differences being unimportant in the far-field compared with the effects of source orientation and vertical uplift. Vertical uplifts are assigned to different intensities in accordance with the convention discussed at the beginning of this section.

Figures 21 and 22 show the Aleutian Trench divided into 12 segments and the Peru-Chile Trench into 3 segments. The segments in the Aleutian Trench were approximately one-quarter the length of the major axis of the standard source, whereas the segments in the Peru-Chile Trench were approximately the length of the major axis of the standard source. The standard source was centered in each segment such that the major axis of the source was parallel to the trench axis. Uplift regions historically have had such an orientation relative to trench systems. The Aleutian Trench is segmented much finer than the Peru-Chile Trench since the Aleutian Trench is oriented relative to the west coast such that elevations produced on the west coast are very sensitive to the exact location of a source along the Trench. Uplifts along the Peru-Chile Trench do not radiate energy directly toward the west coast regardless of their position along the Trench. The Peru and Chile sections of the Peru-Chile Trench have constant orientations relative to the west coast of the United States; therefore, elevations on the west coast are not very sensitive to source location within these sections.

In each of the segments of the Aleutian and Peru-Chile Trenches tsunamis with intensities from 2 to 5 in steps of one-half intensity are generated and propagated across the deep ocean using the deep-ocean numerical model discussed in Chapter II. Tsunamis with intensity less than 2 are too small to produce significant runup on the west coast. An upper limit of 5 was chosen because the largest tsunami intensity ever reported was less than 5 (Soloviev and Go, 1969). Gutenberg and Richter (1965) indicate that there is an upper

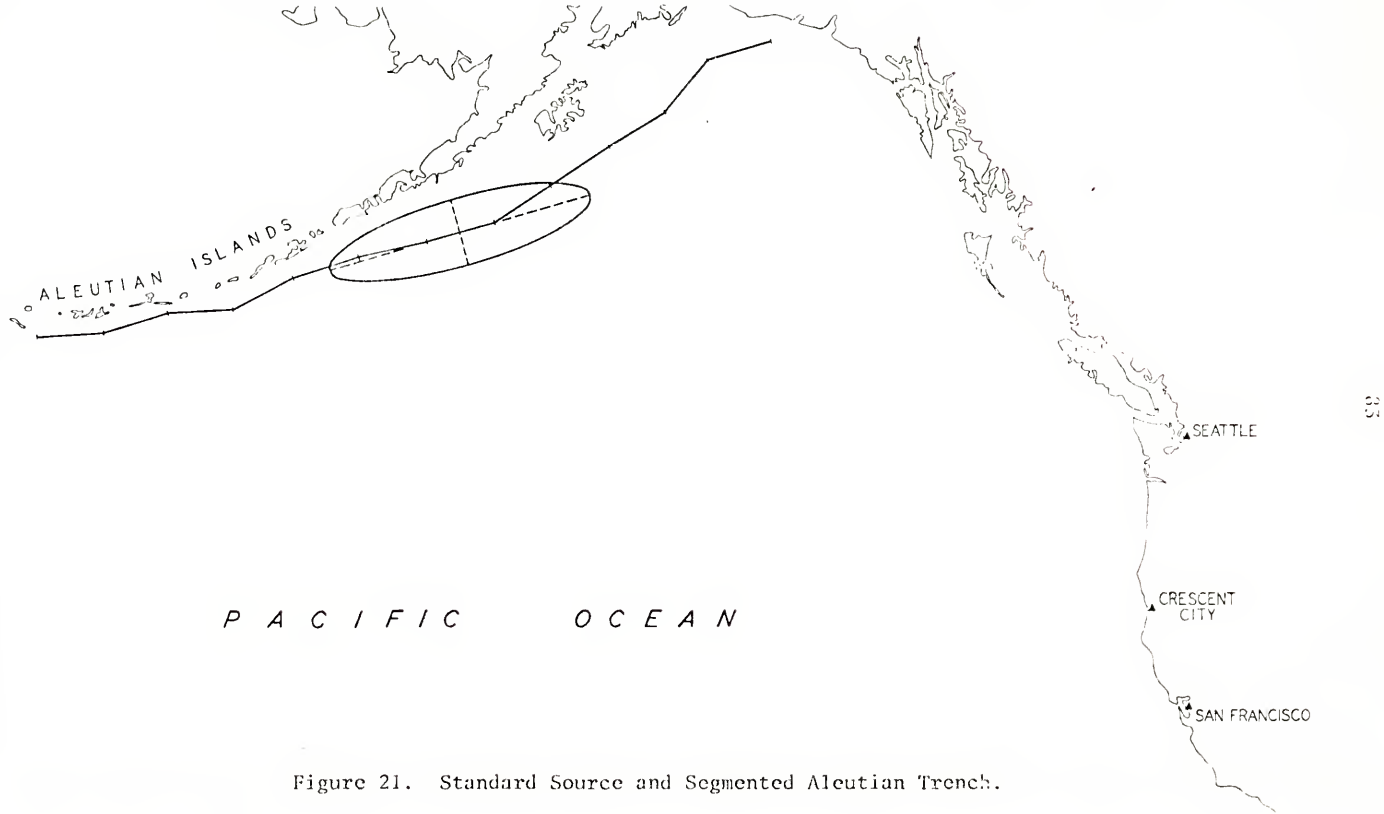

Figure 21. Standard Source and Segmented Aleutian Trench.

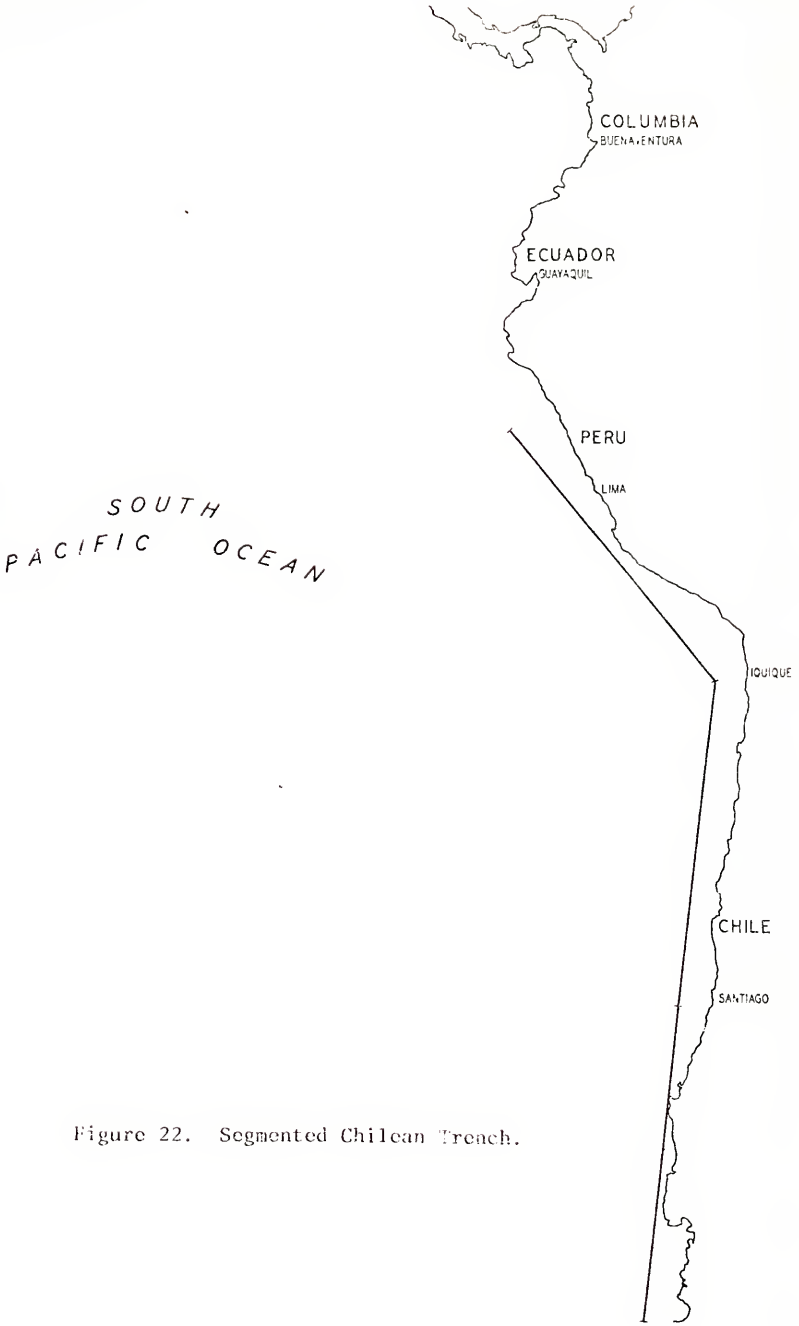

Figure 22. Segmented Chilean Trench.

limit to the strain that can be supported by rock before fracture. Thus, earthquakes only reach certain maximum magnitudes and tsunamis can be expected to have similar upper limits to intensity. Perkins (1972) and McGarr (1976) have demonstrated that future earthquakes cannot have seismic moments (measure of earthquake magnitude for large earthquakes) much larger than those of earthquakes that occurred in recorded history.

The waveforms propagated to the west coast by the deep-ocean model are used as before as input to the nearshore propagation model. Each waveform is propagated from a water depth of 500 meters to shore using the nearshore model and one of the grids shown in Figure 13. Thus, at each grid location on the shoreline of the west coast there is a group of 105 waveforms - seven waveforms (for intensities from 2 to 5 in one-half intensity increments) for each segment of the Aleutian and Peru-Chile Trenches. Each of these waveforms has an associated probability equal to the probability that a certain intensity tsunami will be generated in a particular segment of a trench region.

Effect of the Astronomical Tides

The maximum "still-water" elevation produced during tsunami activity is the result of a superposition of tsunamis and tides. Therefore, the statistical effect of the astronomical tides on total tsunami runup must be included in the predictive scheme presented in this study. Since the waveforms calculated by the nearshore model do not have a simple form (e.g. sinusoidal), the statistical effect of the astronomical tide on tsunami runup must be determined

through a numerical approach. (The effect of the astronomical tides was not considered in the section of predictions for the Hawaiian Islands because the tidal range is quite small for these islands and the local historical data implicitly contain the effects of the tides.)

The waveforms calculated by the nearshore numerical model extend over a period of time of approximately two hours. Three or four wave crests (the largest waves in the tsunami) arrive during this time. Smaller waves arriving at later times, however, often persist for days at a coastal location. An analysis of tide gage records of the 1960 and 1964 tsunamis on the west coast indicates that these smaller waves have amplitudes on the average of 40 percent of the maximum wave amplitude of the tsunami. Therefore, a sinusoidal group of these smaller waves were added to each of the calculated waveforms so that the total waveform extended over a 24 hour period. These smaller waves are important for locations where tsunamis are fairly small compared with tidal variations. At such locations the maximum combined tsunami and astronomical elevation occurs during the maximum tidal elevation.

A computer program was developed to predict time-histories of the astronomical tides at all grid locations on the west coast of the United States. The program was based upon the harmonic analysis methods used in the past by the Coast and Geodetic Survey for mechanical tide-predicting machines (Schureman, 1948). Tidal constants available from the Coast and Geodetic Survey were used as input to the computer program; and a year of tidal elevations was then predicted for grid locations all along the west coast. The year 1964 was

selected because all the major tidal components had a node factor equal to approximately 1.00 during this year making it an average year (node factors can vary by about 10 percent). The node factor is associated with the revolution of the moon's node and has an 18.6-year cycle. Since a tsunami can arrive at any time during this 18.6-year period (arrival at a low of the node factor is equally likely as an arrival at a high), the statistical effect of the varying node factor is small and an average value should be used. The statistical effect of the varying node factor on the predicted runup elevations can be shown to be a small fraction of an inch, using the approach discussed in the next section and Appendix A (with the variance of the nodal variation equal to approximately 0.1 feet squared).

The year of tidal elevations calculated at each of the nearshore numerical model grid points along the west coast was then subdivided into 15-minute segments. The 24-hour waveforms were allowed to arrive at the beginning of each of these 15-minute segments and then superposed upon the astronomical tide for the 24-hour period. The maximum combined tsunami and astronomical tide elevation over the 24-hour period was determined for tsunamis arriving during each of these 15-minute starting times during a year. All of the maximum elevations had an associated probability equal to the probability that a certain intensity tsunami would be generated in a particular segment of the two trench regions and arrive during a particular 15-minute period of a year.

The many maximum elevations with associated probabilities can be used to determine cumulative probability distributions of combined tsunami and astronomical tide elevations. The maximum elevations are ordered and probabilities summed, starting with the largest elevations, until a desired probability is obtained. The elevation encountered when the summed probabilities reach a desired value P is the elevation that is equaled or exceeded with an average frequency of once every 1/P years. Thus, when the summed probabilities reach the value .01, the elevation associated with the last probability summed is the 100-year elevation.

The 100-year and 500-year elevations are determined at all grid points of the nearshore numerical grids using techniques described previously in this chapter. Smooth curves are then used to connect all discrete elevations so that continuous predictions of elevation versus coastline location can be made for all the west coast. Figure 23 shows 100-year and 500-year elevations in the Crescent City, California, area.

Comparison with Local Observation Predictions

Crescent City and San Francisco, California, are the only locations on the portion of the west coast of the United States considered in this study that have sufficient historical data of tsunami activity to allow frequency of occurrence predictions based upon local historical observations. Wiegel (1965) made such predictions of tsunami height (trough to crest height) for Crescent City based upon the period from 1900 to 1965. He predicted 100-year and 500-year heights at Crescent City of approximately 25.6 feet and 43.2 feet,

respectively. If the crest amplitude is taken to be one-half the total height, the 100-year and 500-year elevations are 12.8 feet and 21.6 feet, respectively. However, the crest amplitude at Crescent City is typically greater than one-half the wave height (e.g. the crest amplitude of the largest wave of the 1964 tsunami was approximately 60 percent of the total height). If Wiegel's analysis is applied to historical crest elevations instead of heights, the 100-year and 500-year elevations are found to be 15.4 and 26.4 feet, respectively. Furthermore, the analysis can now be applied to the longer time period from 1900 through 1977. The 100-year and 500-year elevations based upon this longer time span are 14.5 feet and 25.5 feet respectively.

Figure 23 shows 100-year and 500-year elevations of 13.1 feet and 24.9 feet, respectively. These values compare very favorably with the 14.5 feet and 25.5 feet elevations determined from historical data for the period of time from 1900 through 1977. The elevations predicted by the analysis based upon the local historical data are probably somewhat larger than the elevations predicted in this report because the short time period (relative to 100 or 500 years) from 1900 through 1977 includes the exceptionally active years of tsunami generation from 1946 through 1964 (see Chapter III).

The 13.1-foot and 24.9-foot elevations predicted for Crescent City using the techniques discussed in this study are not totally comparable to the elevations predicted using Wiegel's analysis based upon local historical data since the effect of the astronomical tide has been included in the elevations predicted in this study. However,

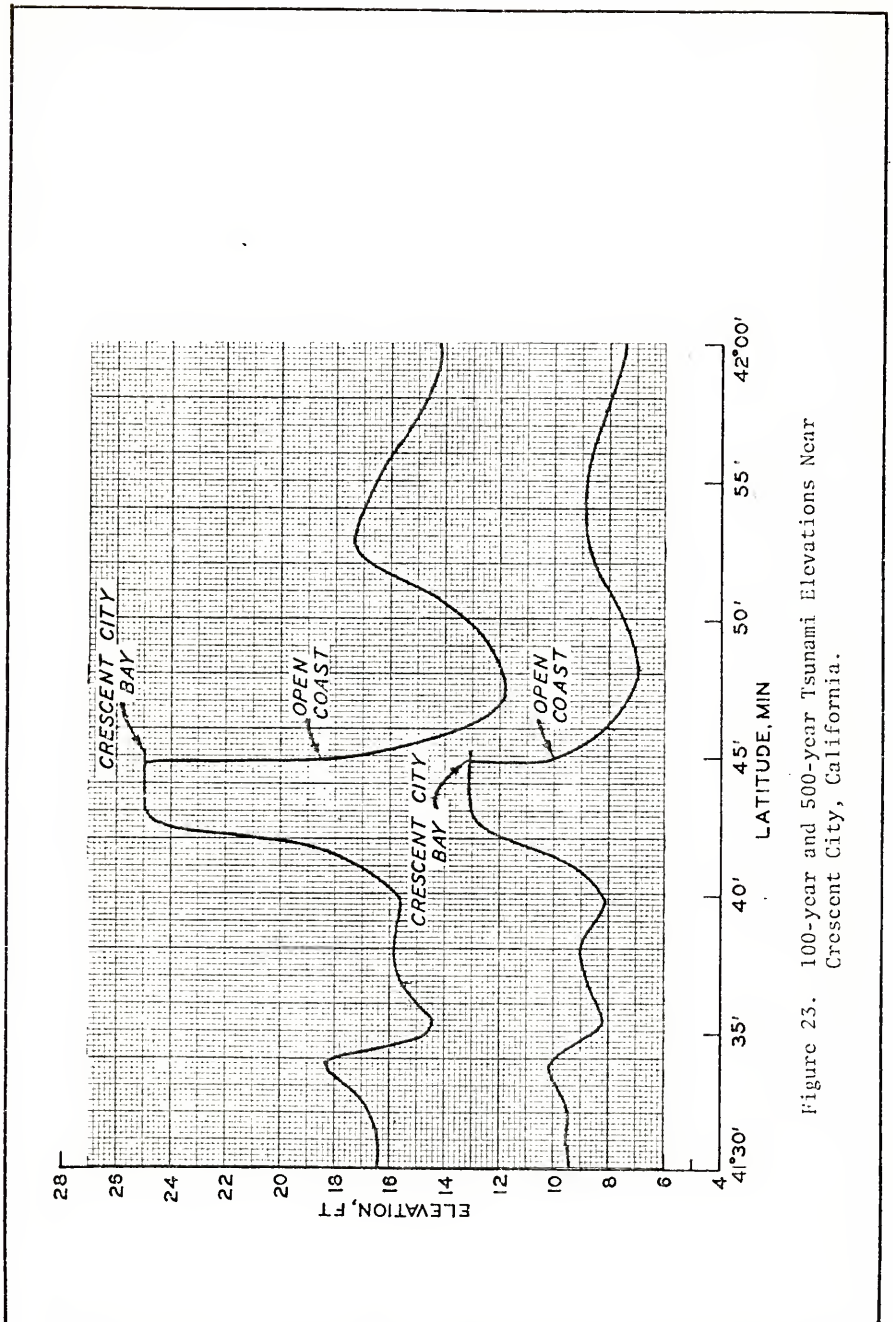

Figure 23. 100-year and 500-year Tsunami Elevations Near Crescent City, California.

the statistical effect of the astronomical tide on the total elevation is not significant at Crescent City due to the large amplitude of tsunamis there. Appendix A shows that the statistical effect of the astronomical tide for a location where tsunamis are large is to increase the predicted elevation by an amount equal to $\frac{\alpha\sigma^2}{2}$, where σ^2 is the tidal variance and equals $\sum_{m=1}^{\infty} C_m^2$, C_m is equal to the m^{th} tidal constituent, and α is given by the following expression (since it was shown earlier in this chapter that elevations are linearly related to the logarithm of probabilities):

$$P(Z) = Ae^{-\alpha Z}$$

with

Z = the elevation above local mean sea level, and

$P(Z)$ = the cumulative probability distribution for the elevation at a given site being equal to or exceeding Z due only to the maximum wave of the tsunami. Based upon the tidal constituents predicted by the Coast and Geodetic Survey, $\sigma^2 = 7.1$ for Crescent City. Using Wiegel's data for the period of time from 1900 through 1977 gives $\alpha = .145$. Therefore, the astronomical tide contributes approximately 0.5 feet to the elevations predicted for Crescent City.

Frequency of occurrence calculations just inside San Francisco Bay were made in an earlier study (Houston and Garcia, 1975) using a simple one-dimensional analytical solution for nearshore propagation. However, portions of San Francisco Bay are included in the nearshore numerical model (see Figure 13) used in this study in order that the effect of the Bay on elevations outside the Bay can be properly

simulated. Thus, approximate elevation calculations can be made in this study at the location of the Presidio tide gage within San Francisco Bay. Figure 24 shows the 100-year and 500-year elevation predictions at the Presidio to be 6.1 feet and 10.0 feet, respectively.

Local historical data of tsunami activity at the Presidio was compiled by Wiegel (1965). Using a logarithmic distribution and Wiegel's wave height data for San Francisco over the period 1900 through 1977 yields 100-year and 500-year heights (trough to crest) of 8.0 feet and 14.2 feet respectively. If the crest amplitude is one-half the height, this yields 100-year and 500-year elevations of 4.0 feet and 7.1 feet respectively. The same analysis based upon data of crest amplitudes yields 100-year and 500-year elevations of 4.4 feet and 7.8 feet, respectively.

It is difficult to compare the elevations predicted using local historical data with the elevations predicted in this study for San Francisco, since the effect of the astronomical tides (included in the calculations of this study) cannot easily be estimated, as was the case for Crescent City. Tsunamis recorded at the Presidio in San Francisco are known to persist at fairly substantial levels for extended periods of time apparently due to an oscillation phenomenon. For example, during the 1964 tsunami there were six waves of approximately equal or greater amplitude than the initial wave (in addition to smaller waves) during the first 8 hours of the tsunami. Oscillations approximately 40 percent of the amplitude of the initial wave persisted for at least another 24 hours. The tidal range at San Francisco is 5.7 feet with mean higher high water (MHHW) 2.7 feet

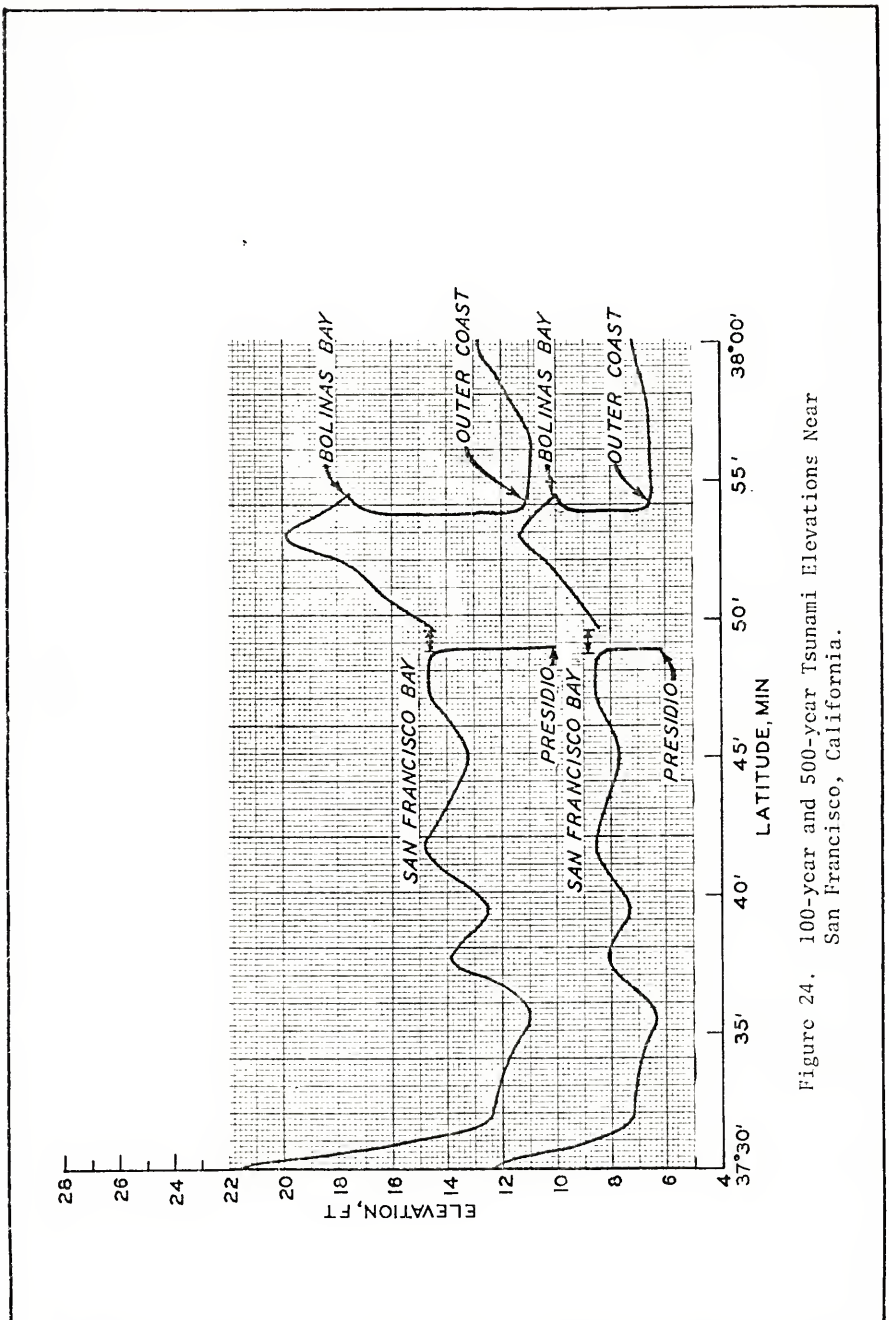

Figure 24. 100-year and 500-year Tsunami Elevations Near San Francisco, California.

above mean sea level (MSL) and mean high water (MHW) 1.0 feet above MSL. At least one of the main waves of a tsunami at San Francisco probably superposes upon either MHW (with the smaller oscillations then adding to MHHW) or MHHW. Thus, the effect of the tides is to contribute 1 to 2.7 feet to the total elevation. These elevations when added to the elevations predicted from local historical data yield 100-year and 500-year elevations of 5.4 feet to 7.1 feet and 8.8 feet to 10.5 feet, respectively. These elevations compare favorably with the 6.1 feet and 10.0 feet elevations determined in this study.

CHAPTER V

CONCLUSIONS

The major objective of the present study has been to determine tsunami elevation frequencies of occurrence at the shoreline for the Hawaiian Islands and the west coast of the continental United States. Numerical models were developed to simulate nearshore tsunami propagation and interaction with coastlines. A finite element numerical model was used to interpolate between modern historical measurements of tsunami elevations in the Hawaiian Islands. Finite difference numerical models were used to propagate tsunamis from the Aleutian-Alaskan and Peru-Chile regions to the west coast of the United States so that frequency of occurrence predictions could be made.

The good agreement between tide gage recordings and numerical simulations of the 1960 Chilean and 1964 Alaskan tsunamis in the Hawaiian Islands indicates that linear, nondispersive, and dissipation-free equations govern nearshore propagation of the main leading waves of long period tsunamis for coastal regions having very short continental shelves. A short continental shelf limits the time available for the development of effects governed by the terms neglected in the equation of motion. Long wave equations that include nonlinear and bottom stress effects were shown to govern propagation of the main leading waves of long period tsunamis over the shallow water region of the west coast of the United States.

Good agreement between the numerical model simulations and tide gage recordings of historical tsunamis confirms the experimental flume tests by Hammack (1972) that showed that the far-field waveform generated by a large impulsive ground displacement does not depend upon the transient motions accompanying the permanent ground motion. The good agreement also shows that the accepted permanent ground deformations of the 1960 Chilean and 1964 Alaskan tsunamis, which were partly measured and partly estimated by Plafker and Savage (1970) and Plafker (1969) respectively, are fairly accurate.

Finally, this study shows that numerical models can be used in conjunction with limited available historical information to make reasonable predictions of tsunami elevations on coastlines. For an area having local historical data of tsunami occurrence, such as the Hawaiian Islands, numerical models can be used to predict elevations at particular locations not having data. For an area lacking almost any local historical data, such as the west coast of the United States, elevation predictions can be made based upon data of tsunami occurrence in tsunamigenic regions and numerical model propagation of tsunamis from generation regions to the area of interest.

APPENDIX

SUPERPOSITION OF LARGE TSUNAMIS AND ASTRONOMICAL TIDES

If the largest wave of a tsunami produces the largest total elevation when the tsunami is superposed upon the astronomical tide (regardless of where the largest wave falls in the tidal cycle), the statistical effect of the astronomical tide on the total elevation can be estimated analytically. Tsunamis satisfy this condition when their maximum waves have amplitudes larger than the sum of the maximum tidal elevation and the elevation of one of the smaller waves which follow the major waves and persist over periods of days.

Let

Z = the elevation at any time above local mean sea level.

$P_S(Z)$ = the cumulative probability distribution for the elevation at a given site being equal to or exceeding Z due only to the maximum wave of the tsunami.

$P_\beta(Z)$ = the probability of the elevation at the same location being equal to or exceeding Z due only to the astronomical tide.

$P(Z)$ = the cumulative probability distribution for the elevation at a given site being equal to or exceeding Z due to the maximum wave of the tsunami and the astronomical tide.

According to Chandrasekhar (1943), $P(Z)$ can be calculated from the equation

$$P(Z) = \int_{-\infty}^{\infty} f_\beta(\lambda) P_S(Z-\lambda) d\lambda \qquad \text{(A1)}$$

where

$$f_\beta(Z) = -\frac{dP_\beta(Z)}{dZ}$$

and $f_\beta(Z)$ is the probability density for the astronomical tide.

$P_\beta(Z)$ can be approximated by a Gaussian distribution.

Therefore,

$$f_\beta(Z) = \frac{1}{\sqrt{2\pi}\,\sigma} e^{-Z^2/2\sigma^2} \tag{A2}$$

where the variance is

$$\sigma^2 = \sum_{m=1}^{\infty} C_m^2$$

and C_m equals the m^{th} tidal constituent.

$P_S(Z)$ can be approximated by an exponential function (see Chapter II) as follows:

$$P_S(Z) = Ae^{-\alpha Z} \tag{A3}$$

Substituting Equations (A2) and (A3) into (A1) and performing the integration yields

$$P(Z) = Ae^{-\alpha\left(Z - \frac{\alpha\sigma^2}{2}\right)}$$

or

$$P(Z) = Ae^{-\alpha Z^1}$$

where

$$Z^1 = Z - \frac{\alpha\sigma^2}{2} .$$

Thus, the net effect of the astronomical tide is to produce a P(Z) identical with $P_S(Z)$ except for a shift of Z by an amount $\frac{\alpha\sigma^2}{2}$. The variance σ^2 can be determined for locations in the United States from tidal harmonic coefficients available from the Coast and Geodetic Survey. The exponential constant α in Equation (A3) is obtained from a least-squares exponential fit of tsunami elevation data at a location.

REFERENCES

Adams, W. M., 1970: Tsunami effects and risk at Kahuku Point, Oahu, Hawaii. Engineering Geology Case Histories, Geo. Soc. of Amer., No. 8, 63-70.

Adams, W. M., 1975: Conditional expected tsunami inundation for Hawaii. J. of Waterways, Harbors, and Coastal Eng. Div., Amer. Soc. Civ. Eng., 101, No. WW4, 319-329.

Bernard, E. N. and A. C. Vastano, 1977; Numerical computation of tsunami response for island systems. J. of Phys. Oceanogr., 7, 389-395.

Borgman, L. E. and D. T. Resio, 1977: Extremal prediction of wave climatology. Ports 77, 4th Ann. Symp. of the Waterways, Port, Coastal, and Ocean Div., Amer. Soc. Civ. Eng., 1, 394-412.

Carrier, G. F., 1966: Gravity waves on water of variable depth, J. of Fluid Mech., 24, Pt. 4, 641-659.

Chandrasekhar, S., 1943: Stochastic problems in physics and astronomy. Rev. of Mod. Phys. 15, 1-89.

Chen, H. S. and C. C. Mei, 1974: Oscillations and wave forces in an offshore harbor. Rept. No. 190, Mass. Inst. of Tech., Cambridge, Mass., 215 pp.

Cole, R. A. and P. J. Riech, 1976: Computer program for drawing finite element grids. Tech. Rept. N-76-2, U. S. Army Eng. Waterways Exp. Sta., Vicksburg, Miss. 110 pp.

Courant, R., 1943: Variational methods for the solution of problems of equilibrium and vibration. Bull. of the Amer. Math. Sec., 49, 1-23.

Cox, D. C., 1964: Tsunami height-frequency relationship of Hilo. Nov. 1964, Hawaii Inst. of Geophys., Univ. of Hawaii, Honolulu, Hawaii, 7 pp.

Der Kiureghian, A. and A. H-S. Ang, 1977: A fault-rupture model for seismic risk analysis. Bull. of the Seis. Soc. of Amer., 64, No. 4, 1173-1194.

Desai, C. S. and J. F. Abel, 1972: Introduction to the Finite Element Method; A Numerical Method for Engineering Analysis, Van Nostrand Reinhold Co., 477 pp.

Dronkers, J. J. 1964: Tidal Computations in Rivers and Coastal Waters, North-Holland Publishing Co., Amsterdam, 518 pp.

Eaton, J. P., D. H. Richter, and W. V. Aults, 1961: The tsunami of May 23, 1960, on the island of Hawaii. Bull. of the Seis. Soc. of Amer., 51, No. 2, 135-157.

Grace, R. A., 1969: Reef runway hydraulic model study: Honolulu International Airport, three-dimensional tsunami study. Dept. of Transp., St. of Hawaii, Honolulu, 23 pp.

Gumbel, E. J., 1955: The calculated risk in flood control, App. Sci. Res., 5, Sec. A, 273-280.

Gutenberg, B. and C. F. Richter, 1965: Seismicity of the Earth and Associated Phenomena, 2nd ed., Hafner Publishing Co., 310 pp.

Hall, J. V. and G. M. Watts, 1953: Laboratory investigation of the vertical rise of solitary waves on impermeable slopes; Tech. mem. 33, U. S. Corps of Eng., Beach Erosion Board, 75 pp.

Hammack, J. L., 1972: Tsunamis; a model of their generation and propagation. Rept. No. KH-R-28, Calif. Inst. of Tech. Pasadena, Calif., 261 pp.

Hammack, J. L., and H. Segur, 1977: Modeling criteria for long water waves. Univ. of Fla., Gainesville, Fla. (to be published).

Hatori, T., 1963: Directivity of tsunamis; Bull. of the Earthquake Res. Inst., Univ., of Tokoyo, 41, 61-81.

Heitner, K. L. and Housner, G. W., 1970: Numerical model for tsunami runup. J. of the Waterways, Harbors, and Coastal Eng. Div., Amer. Soc. Civ. Eng. 96, No. WW3, 701-719.

Hom-ma, S., 1950: On the behavior of seismic sea waves around a circular island. Geophys. Mag., 21, 199-208.

Houston, J. R., R. D. Carver, and D. G. Markle, 1977: Tsunami-wave elevation frequency of occurrence for the Hawaiian Islands. Tech. Rept. H-77-16, U. S. Army Eng. Waterways Exp. Sta., Vicksburg, Miss., 109 pp.

Houston, J. R. and A. W. Garcia, 1974: Type 16 flood insurance study: tsunami predictions for Pacific coastal communities. Tech. Rept. H-74-3, U. S. Army Eng. Waterways Experiment Sta., Vicksburg, Miss., 128 pp.

Houston, J. R. and A. W. Garcia, 1975: Type 16 flood insurance study: tsunami predictions for Monterey and San Francisco Bays and Puget Sound. Tech. Rept. H-75-17, U. S. Army Eng. Waterways Exp. Sta., Vicksburg, Miss., 263 pp.

Houston, J. R., R. W. Whalin, H. L. Butler, D. Raney, 1975 a: Probable maximum tsunami runup for distant seismic events NORCO-NP-1, PSAR, Fugro Inc., Long Beach, Calif., 253 pp.

Houston, J. R., R. W. Whalin, A. W. Garcia, H. L. Butler, 1975 b: Effect of source orientation and location in the Aleutian Trench on tsunami amplitude along the Pacific coast of the continental United States. Res. Rept. H-75-4, U. S. Army Eng. Waterways Exp. Sta., Vicksburg, Miss., 48 pp.

Hwang, L. S., H. L. Butler, and D. J. Divoky, 1975: Tsunami model: generation and open-sea characteristics. Bull. of the Seis. Soc. of Amer., 62, No. 6, 1579-1596.

Hwang, L. S. and D. Divoky, 1975: Numerical investigations of tsunami behavior. Tetra Tech, Inc., Pasadena, Calif., 37 pp.

Jordaan, J. M. and W. M. Adams, 1968: Tsunami height, Oahu, Hawaii: Model and nature. Proc. of the Eleventh Conf. on Coastal Eng., Inst. of Civ. Eng. and the Amer. Soc. of Civil Eng., 1555-1574.

Kanamori, H., 1977: The energy release in great earthquakes. J. of Geophys. Res., 82, No. 20, 2981-2987.

Kaplan, K., 1955: Generalized laboratory study of tsunami runup. Tech. Memo. No. 60, U. S. Army Corps of Eng., Beach Erosion Board, 30 pp.

Kelleher, J., J. Savino, H. Rowlett, and W. McCann, 1974: Why and where great thrust earthquakes occur along island arcs. J. of Geophys. Res., 79, No. 32, 4889-4899.

Keller, J. B. and H. B. Keller, 1964: Water wave run-up on a beach. Service Bureau Corp., New York, 34 pp.

Kishi, J. and H. Saeki, 1966: The shoaling, breaking, and runup of solitary waves on impermeable rough slopes. Proceed. of the Tenth Conf. on Coastal Eng., Amer. Soc. of Civ. Eng., 1, 322-348.

Leendertse, J. J., 1967: Aspects of a computational model for long-period water-wave propagation. Eme. Rm-5294-PR, Rand Corp., Santa Monica, Calif., 165 pp.

Loomis H. G. 1970: A method of setting up the eigenvalue problem for the linear, shallow water wave equation for irregular bodies of water with variable water depth and application to bays and harbors in Hawaii. NOAA-JTRE-16, Hawaii Inst. of Geophys., Univ. of Hawaii, Honolulu, Hawaii, 77 pp.

Loomis, H. B. 1976: The tsunami of November 29, 1975 in Hawaii, HIG-75-21, Hawaii Inst. of Geophys., Univ. of Hawaii, Honolulu, Hawaii, 95 pp.

McGarr, A., 1976: Upper limit to earthquake size. Nature, 262, No. 5567, 378-379.

Mader, C. L., 1974: Numerical simulation of tsunamis. J. of Phys., 4, 74-82.

Madsen, O. S. and C. C. Mei, 1969: The transformation of a solitary wave over an uneven bottom. J. of Fluid Mech., 39, 781-791.

Magoon, O. T., 1965: Structural damage by tsunamis. Coastal Eng. Santa Barbara Spec., Conf., Amer. Soc. of Civ. Eng. 35-68.

Mei, C. C., 1978: Numerical methods in water-wave diffraction and radiation. Ann. Rev. of Fluid Mech., 10.

Mei, C. C. and B. LeMehaute, 1966: Note on the equations of Long waves over an uneven bottom. J. of Geophys. Res., 71, 2.

Newmark, N. M. and E. Rosenblueth, 1971: Fundamentals of Earthquake Engineering, Prentice-Hall, 528 pp.

Noye, B. J., 1970: The frequency response of a tide-well: Proc. of the Third Australasian Conf. on Hyd. and Fluid Mech., Inst. of Eng., Sydney, Australia, No. 2630.

Omer, G. C. and H. H. Hall, 1949: The scattering of tsunamis by a cylinderical island. Bull. Seis. Soc. Amer., 39, 257-260.

Parraras-Carayannis, G., 1977: Catalog of tsunamis in Hawaii. Rept. SE-4, World Data Center A for Solid Earth Geophysics, Boulder, Colo., 77 pp.

Peregrine, D. H., 1967: Long waves on a beach. J. of Fluid Mechanics, 27, pt. 4, 815-827.

Perkins, D., 1972: The search for maximum magnitude. Nat. Oceanogr. and Atmos. Admin. Earthquake infor. Bull., July, 1972, 18-23.

Plafker, G., 1969: Tectonics of the March 27, 1964, Alaskan earthquake. U. S. Geological Survey Professional Paper, 543-I, 11-174.

Plafker, G. and J. C. Savage, 1970: Mechanism of the Chilean earthquake of May 21 and 22, 1960. Bull. of Geo. Soc. of Amer., 81 No. 4, 1001-1030.

Platzman, G. W., 1958: A numerical computation of the surge of 26 June 1954 on Lake Michigan. Geophysica, 6, 409-438.

Raney, D. C., 1976: Numerical analysis of tidal circulation for Long Beach Harbor-existing conditions and alternate plans for Pier J completion, Misc. Paper H-76-4, U. S. Army Eng. Waterways Exp. Sta., Vicksburg, Miss., 138 pp.

Rascon, O. A. and A. G. Villarreal, 1975: On a stochastic model to estimate tsunami risk. J. of Hyd. Res., 13, No. 4, 383-405.

Savage, R. P., 1958: Wave run-up on roughened and permeable slopes. J. of Waterways and Harbors Div., Amer. Soc. of Civ. Eng., 84, No. WW3, 1640-1641.

Saville, T., 1956: Wave run-up on shoreline structures. J. of Waterways and Harbors Div., Amer. Soc. of Civ. Eng., 82, No. WW2, 925-950.

Schureman P., 1948: Manual of harmonic analysis and prediction of tides. Spec. Public 86, U. S. Coast and Geod. Sur., Washington, D. C. 317 pp.

Soloviev, S. L., 1969: Recurrence of tsunamis in the Pacific. Proc. of the Inter. Symp. on Tsunamis and Tsunami Res., 35-63.

Soloviev, S. L. and No. Go, 1969: Catalog of Tsunamis in the Pacific (Main Data), in Russian, Union of Soviet Socialist Republics, Moscow.

Strang, G. and G. J. Fix, 1973: An Analysis of the Finite Element Method, Prentice-Hall, 328 pp.

Svendsen, I. A., 1974: Cnoidal waves over a gently sloping bottom. Inst. of Hydrodyn. and Hydr. Eng., Univ. of Denmark, Lyngby, Denmark, 181 pp.

Takahasi, R. 1964: Coastal effects upon tsunamis and storm surges. Bull. of the Earthquake Res. Inst., Univ. of Tokoyo, 42, 175-180.

Tilling, R. I., R. Y. Koyanagi, R. W. Lipman, J. P. Lockwood, J. G. Moore, and D. A. Swanson, 1976: Earthquake and related catastrophic events; island of Hawaii, November 29, 1975: a preliminary report. Geological Survey Circular, No. 740, U. S. Geological Survey, Arlington, Virginia, 33 pp.

Towill Corp., 1975: Tsunami studies for Oahu, Hawaii. Towill Corp., Honolulu, Hawaii, 38 pp.

Turner, M. J., R. W. Clough, H. C. Martin, and L. P. Topp, 1956; Stiffness and deflection analysis of complex structures, J. of the Aeronautical Sci., 23, No. 9, 805-823, 854.

Ursell, F., 1953: The long-wave paradox in the theory of gravity waves. Proceedings, Cambridge Philsophical Society, 49, 685-694.

Van Dorn, W. G., 1970: Tsunami response at Wake Island: A model study. J. Mar. Res., 28, 336-344.

Vastano, A. C. and E. N. Bernard, 1973: Transient long wave response for a multiple island system. J. Phys. Oceanogr., 3, 406-418.

Vastano, A. C. and R. O. Reid, 1966: A numerical study of the tsunami response of an island. Ref. 66-26T, Dept. of Oceanography, Texas A&M University, 141 pp.

Wiegel, R. L., 1965: Protection of Crescent City, California from tsunami waves. Redevelopment Agency of the City of Crescent City, 114 pp.

Wilson, B. W., 1959: Earthquake occurrence and effects in ocean area. CR 69.027, Naval Civ. Eng. Lab., Port Hueneme, Calif., 118 pp.

Wilson, B. W. and A. Torum, 1968: The tsunami of the Alaskan earthquake, 1964: engineering evaluation, Tech. Mem. 25, U. S. Army Coastal Eng. Research Center, Washington, D. C., 401 pp.

Wybro, P. G., 1977: M. S. Plan B, Univ. of Hawaii, Honolulu, Hawaii, (to be published).

Zienkiewicz, O. C. and Y. K. Cheung, 1966: Finite elements in the solution of field problems. The Engineer, 507-510.

Zienkiewicz, O. C., 1971: The finite element method in engineering science, 2d. ed., McGraw Hill, 521 pp.

BIOGRAPHICAL SKETCH

James Robert Houston was born in Berkeley, California, on March 31, 1947. He was awarded a Bachelor of Arts degree in Physics at the University of California at Berkeley in June 1969 and a Masters of Science degree in Physics at the University of Chicago in June 1970. His doctoral studies at the University of Chicago were interrupted in November 1970 when he was inducted into the U. S. Army. For a year and a half he was involved in the study of explosively generated water waves in the Nuclear Weapons Effects Laboratory of the U. S. Corps of Engineers Waterways Experiment Station in Vicksburg, Mississippi. Following an honorable discharge from the U. S. Army in May 1972, he was engaged as a Research Physicist by the Wave Dynamics Division, Hydraulics Laboratory, Waterways Experiment Station. In September 1974, he was awarded a Master of Science degree in Coastal Engineering at the University of Florida. He is the author of several reports and papers dealing with numerical investigations of long wave phenomena.

I certify that I have read this study and that in my opinion it conforms to acceptable standards of scholarly presentation and is fully adequate, in scope and quality, as a dissertation for the degree of Doctor of Philosophy.

Knox Millsaps, Chairman
Professor and Chairman of Engineering Sciences

I certify that I have read this study and that in my opinion it conforms to acceptable standards of scholarly presentation and is fully adequate, in scope and quality, as a dissertation for the degree of Doctor of Philosophy.

Joseph L. Hammack, Cochairman
Associate Professor of Engineering Sciences

I certify that I have read this study and that in my opinion it conforms to acceptable standards of scholarly presentation and is fully adequate, in scope and quality, as a dissertation for the degree of Doctor of Philosophy.

D. M. Sheppard
Associate Professor of Coastal and Oceanographic Engineering and Engineering Sciences

I certify that I have read this study and that in my opinion it conforms to acceptable standards of scholarly presentation and is fully adequate, in scope and quality, as a dissertation for the degree of Doctor of Philosophy.

M. A. Eisenberg
Professor of Engineering and Engineering Sciences

I certify that I have read this study and that in my opinion it conforms to acceptable standards of scholarly presentation and is fully adequate, in scope and quality, as a dissertation for the degree of Doctor of Philosophy.

Michael E. Thomas
Professor and Chairman of Industrial and Systems Engineering

This dissertation was submitted to the Graduate Faculty of the College of Engineering and to the Graduate Council, and was accepted as partial fulfillment of the requirements for the degree of Doctor of Philosophy.

June 1978

Dean, College of Engineering

Dean, Graduate School

UNIVERSITY OF FLORIDA
3 1262 08553 2686